2015

THE EFFECT OF IMMEDIATE SALINE WATER CURING ON THE STRENGTH, COMPOSITION, AND MICROSTRUCTURE OF GEOPOLYMER CEMENT

Lindsay Duran

THE EFFECT OF IMMEDIATE SALINE WATER CURING ON THE STRENGTH, COMPOSITION, AND MICROSTRUCTURE OF GEOPOLYMER CEMENT

A Master of Science Project

By

Lindsay E. Duran

Department of Civil and Environmental Engineering
University of Massachusetts Amherst
Amherst, MA 01003

MASTER OF SCIENCE IN CIVIL ENGINEERING

MAY 2015

The Effect of Immediate Saline Water Curing on the Strength, Composition, and Microstructure of Geopolymer Cement

A Masters Project Presented

by

Lindsay E. Duran

Approved as to style and content by:

Guoping Zhang , Chairperson

Don J. DeGroot, Member

Sanjay Arwade
Civil and Environmental Engineering Department

DEDICATION

To my grandmother, R. Florence Dillon.

ACKNOWLEDGMENTS

I would like to acknowledge the support, guidance, and friendship of the following people and groups who assisted me without hesitance throughout my entire graduate study.

Guoping Zhang, Academic Advisor and Committee Chair, for his guidance, support, and encouragement throughout my graduate career.

Don J. DeGroot, Committee Member, for his guidance and assistance throughout my project.

The Civil and Environmental Engineering Department staff that assisted me throughout my academic career, with a special thanks to Jodi Ozdarski, Kelly Ives, and Jennifer Pease.

Dale Renfrow, from the Smith College Center for Design and Fabrication, Pete Dawson from the Geoscience Department, Louis Raboin and Alexander Ribbe from the W.M.. Keck Electron Microscopy Center, and Steven Rudolph and Chunwei Ge from the Massachusetts Institute of Technology Department of Civil and Environmental Engineering for assisting me in the various aspects of fabrication and testing.

The past and present graduate students, with a special thanks to Will Lukus for taking me under his wing and helping me learn the ropes when I began my project.

The Bill & Melinda Gates Foundation, the National Science Foundation, and McMillen Jacobs Associates for providing me with the funds to pursue my graduate studies and research.

Lastly, to my family and friends who encouraged me to keep trying my best and to work to overcome any hardship I encountered in my academic career. Their loving support, belief, and encouragement are the means by which I got to where I am today.

ABSTRACT

THE EFFECT OF IMMEDIATE SALINE WATER CURING ON THE STRENGTH, COMPOSITION, AND MICROSTRUCTURE OF GEOPOLYMER CEMENT

May 2015

Lindsay E. Duran, B.S., Smith College

M.S., University of Massachusetts Amherst

Directed by: Dr. Guoping Zhang

The low durability and low resistance of ordinary Portland cement led to an investigation into the viability of geopolymer cement as an alternative to well cement for soil improvement in saline environments and well cement in offshore drilling and carbon sequestration projects. This thesis presents the results of a laboratory investigation into the effect of immediate saline water curing on the strength, composition, and microstructure of geopolymer cement. The experimental program began with preliminary work in designing adequate geopolymer cement and developing a curing environment that simulates offshore or underground conditions and facilitates immediate curing of cement specimens. Pure geopolymer cement with a Si/Al ratio of 1.78 was synthesized from an admixture of Class C fly ash and metakaolin and immediately cured in saline water of 0, 15, and 35 ppt concentrations. After 28 days of water curing, the specimens were removed from their curing environments and characterized for strength, composition, and microstructure. Class G well cement specimens were simultaneously cured under similar conditions and analyzed as a source of comparison. Results indicate

that the strength of the geopolymer cement increases with increasing salinity, while the Class G cement exhibits opposite behavior. Mineralogical compositional analysis (X-ray diffraction) demonstrates the formation of a geopolymer through alkali activation of amorphous silica and alumina. Chemical compositional analyses (pH, X-ray fluorescence) revealed an increased rate of chemical exchange between the cement slurry and curing water occurred with decreasing salinity for both cement types. The microstructural characterization was carried out using scanning electron microscopy and energy dispersive X-ray spectroscopy. The geopolymer cements possessed nanoporosity and observed reacted product that was independent of curing salinity. All of the findings suggest that geopolymer cement derived from an admixture of metakaolin and Class C fly ash would be a viable alternative to ordinary Portland cement in well cementing applications.

TABLE OF CONTENTS

LIST OF TABLES

Table **Page**

LIST OF FIGURES

Figure **Page**

LIST OF SYMBOLS

Symbol	Units	Description
w	%	Moisture content
W_{wet}	g	Wet weight of cement specimen
W_{dry}	g	Dry weight of cement specimen
ρ	g/cm^3	Bulk density
V_T	cm^3	Total volume of cement specimen
θ	°	Diffraction angles
e_a	%	Axial strain
σ	MPa	Compressive Strength
e_f	%	Failure Strain
σ_f	MPa	Peak Compressive Strength
E	GPa	Young's Modulus

LIST OF ABBRIEVIATIONS

Abbreviation	Meaning
OPC	Ordinary Portland cement
API	American Petroleum Institute
ASTM	American Society for Testing and Materials
ISO	International Standard Organization
LOI	Loss on ignition
XRF	X-ray fluorescence
CFA	Class C fly ash
MK	Metakaolin
PPT	Parts per thousand
XRD	X-ray diffraction
SEM	Scanning electron microscope
EDS	Energy dispersive X-ray spectroscopy

1 INTRODUCTION

1.0 General

Concrete is one of the most utilized construction materials in the world. Durability and acid resistance are desired properties of concrete and cement used for onshore and offshore applications. Portland cement is typically the cementitious binder used by the community in concrete. If designed properly, it can exhibit excellent strength and durability and is considered an adaptable material that is commonly available and affordable. A draw back to Portland cement is that there are many environment issues associated with its production. Extremely large amounts of natural resources are required to produce the billions of tons of concrete each year. Approximately one ton of carbon dioxide (CO_2) is released for every ton of Portland cement that is produced during the manufacturing process. This is primarily due to the calcination of limestone and combustion of fossil fuel. Worldwide, the cement industry alone is responsible for approximately 5-7% of global anthropogenic carbon emissions [Huntzinger et al. 2009; Meyer 2009].

The desire to alleviate the stress placed on the natural resources used in the manufacture of Portland cement, lower construction cost, and improve workability, mechanical, and durability properties led to the utilization of industrial byproducts and other materials in concrete. These additives include silica fume, ground granulated blast furnace slag, fly ash and other calcined pozzolanic materials such as metakaolin [Li et al 2003; Atis et al. 2009; Melo et al. 2010; Mohammed et al. 2011; Sumer 2012]. Fly ash is a by-product of burning coal and is available in a low calcium (Class F) and high calcium

(Class C) composition. It has been established that fly ash induces noteworthy increase in workability and long-term strength. In addition to this, fly ash has also proven to produce concrete with low permeability [Chung et al. 2010].

The main role of fly ash in concrete consists of three aspects; the morphologic effect, the micro aggregate effect and the pozzolanic effect. The morphologic effect is responsible for the increased workability of the cement and states that there are many micro beads in fly ash that act as a lubricant when incorporated into fresh concrete. The increased density is partially due to the micro aggregate effect, which states that the micro beads are able to disburse well and combine securely with the gel formed during the cement hydration. The main benefit of fly ash is attributed to the pozzolanic effect. This effect states that the unfixed aluminum oxide (Al_2O_3) and silicon dioxide (SiO_2) in fly ash can be activated by the calcium hydroxide ($Ca(OH_2)$) product of the cement hydration and produce more hydrated calcium silica hydrate (C-S-H) gel. This hydrated gel can fill up the capillary in concrete, resulting in an increase in concrete strength [Cao et al. 2000].

An alternative to Portland cement that can also utilize the benefits of fly ash is geopolymer cement. A geopolymer is an alkali-activated cementitious binder that is derived from aluminosilicate-bearing raw materials. The three most common classes of raw materials utilized in geopolymerization are slags, calcined clays, and coal fly ashes. In previous studies, it had been found that geopolymer cement would be an excellent replacement for ordinary Portland cement (OPC). Geopolymer cement has proven to possess excellent strength, acid resistance, and durability when compared to OPC. In addition to this, there is less CO_2 generated during the production of geopolymer cement

when compared to the production of OPC. Kaolin based-geopolymeric cement generates six times less CO_2, from combustion-fuel, compared to OPC. Fly ash based-geopolymeric cement generates up to nine times less CO_2 compared to OPC [Davidovits, 2008].

1.1 Fly Ash-Based Geopolymer Cement as Well Cement

In today's society, great effort had been made to embrace renewable energy as a competitor to the nonrenewable energy market. Incentives have been issued to encourage the switch to renewable energy resources. However, even in a society that is more aware of the carbon footprint and the repercussions of advancing without reformation, fossil fuels are still the primary energy source. Greenhouse gases, such as carbon dioxide, methane, nitrous oxide, etc., are emitted from the combustion and calcination of fossil fuels to the atmosphere [Sanna et al. 2012]. These gases pose a serious environmental problem. It has been reported that CO_2 contributes to 55% of global warming [Yeh et al. 1999]. One effective method of reducing CO_2 emissions is capturing and injecting CO_2 deep underground into reservoirs such as saline aquifers, coal seams, and depleted oil and gas reservoirs [Bruant et. al, 2002]. This method is referred to as carbon sequestration.

In order for carbon sequestration projects to be successful, the well cement used between the casing and caprock and the inside of the casing must provide the appropriate zonal isolation. Degradation of the cement poses a threat to the overall safety of the project and can lead to gas leakage through the wellbore. For petroleum/oil well sealing and carbon sequestration projects, it is common practice to use American Petroleum Institute (API) recommended class 'G' and 'H' Portland cement.

Studies into the suitability of fly ash geopolymer cement as well cement in CO_2 sequestration wells have largely focused on utilizing American Society for Testing and Materials (ASTM) Class F fly ash due to its availability [Nasvi et al. 2012; Nasvi et al. 2013]. In addition to this research, many previous studies investigate the impact of curing environment on the strength and overall durability of geopolymer derived cement. However, none truly look into the effect on immediate curing of a geopolymer in saline water environments.

Due to the increased use of lignite and subbituminous coals, there has been a large increase in the availability of ASTM Class C fly ash. The increase in availability and the deficit in publications regarding Class C fly ash geopolymers act as a motivation to further research into the behavior of a Class C fly ash geopolymer cement in environments that simulate those of oil well cements.

In this study, geopolymer derived cement was created from ASTM Class C fly ash and metakaolin, poured into a curing apparatus, and cured in varying saline water environments for 28 days. A porous mold was developed as a curing apparatus to allow for saline water to access the geopolymer cement, while containing the cement's solid components during early curing. The resulting impact of immediate saline water curing on unconfined compressive strength, composition and microstructure was then analyzed.

1.2 Objectives of Research

As mentioned earlier, the present study investigates the effects of immediate saline water curing on the unconfined compressive strength and structural integrity

geopolymer derived cement. This research program provided an opportunity to assess the viability of high calcium ASTM Class C fly ash and metakaolin-derived geopolymer cement as an alternative to API Class G and H Portland cement. These cements are typically utilized in offshore oil well sealing and carbon sequestration projects. Over the years, geopolymer technology has proven to exceed Portland cement in many ways. The laboratory test program was also performed to support the quest of identifying "greener" and more cost effective construction materials.

The objectives of the research are:

1. To develop a design mixture for a Class C fly ash and metakaolin-derived geopolymer cement that is both workable and exhibits excellent hardened strength.
2. To develop a curing process that simulates immediate curing within a saline water environment.
3. To identify the effect of immediate saline water curing on the compressive strength, composition and microstructural behavior of the cement.
4. To compare the behavior of the geopolymer cement to API Class G oil well cement.

1.3 Scope of Research

The research utilized high calcium ASTM Class C fly and metakaolin for making geopolymer cement. The scope of the research involved designing an adequate geopolymer design mix, developing a curing apparatus in which the geopolymer

specimens could undergo immediate curing in various saline water environments and assessing the unconfined compressive strength, composition and microstructural characteristics after 28 days of immediate saline water curing.

1.4 Organization of Thesis

Chapter 2 presents a background review of relevant literature pertaining to the justification of this research and unconfined compressive strength of geopolymers. It includes information on Portland cement, blended cements, fly ash, and an introduction into geopolymers.

Chapter 3 presents the experimental program followed in this study. It includes information on the materials used, preliminary lab work, experimental setup, and methods testing/analysis.

Chapter 4 presents the experimental analysis of compressive strength. This includes methods of testing, sample preparation, results of testing, and general conclusions.

Chapter 5 presents experimental analysis of elemental and mineralogical composition. This includes the methods of analysis, sample preparation, results, and general conclusions.

Chapter 6 presents the experimental analysis of microstructure. This includes methods of analysis, sample preparation, analytical results, and general conclusions.

Chapter 7 presents the overall conclusions based on the results and recommendations for future work.

2 LITERATURE REVIEW

2.0 Introduction

The following sections present information on Portland cements (2.1), blended cements (2.2), and fly ash (2.3), in addition to a detailed introduction to geopolymers, their components, and additional background required to develop fly ash/metakaolin-based geopolymer cement (2.4).

2.1 Specifications for Portland Cements

Concrete is a composite material that is composed of water, an aggregate, and cement. The cementitious binder commonly used for concrete is Portland cement. Portland cements, depending on their application, are modified by the raw materials and the process used to combine them in order to meet certain chemical and physical standards. Specifications for the manufacture of Portland cement are imposed by various agencies. The American Society for Testing and Materials (ASTM) primarily deals with cements that are used for construction, while the American Petroleum Institute (API) and the International Standard Organization (ISO) write specifications for cements used only in wells. Cements used in wells require different specifications because they are exposed to conditions that are not encountered in construction.

ASTM C150 provides specifications for eight types of Portland cement [ASTM 2002]. The types of Portland cement are Type I, IA, II, IIA, III, IIIA, IV and V. The standard defines Portland cement as “hydraulic cement”, cement that hardens by reacting with water and forms a water-resistant product. The composition of each of the eight

types of Portland cement is limited to the following ingredients: aluminum oxide, ferric oxide, magnesium oxide, sulfur trioxide, tricalcium silicate, dicalcium silicate, tricalcium aluminate, and tetracalcium aluminofernite. The "A" designation specifies air-entraining cements. Cement types I, II, and III can also come with an "MH" designation. This is for when moderate heat of hydration is required for the cement. Out of the eight types of Portland cement specified by this standard, Types I and II are the most commonly used.

API Specification 10A/ISO10426 provides specifications for cements and materials for well cementing [API 2010]. The specifications cover six classes of well cements and provide chemical and physical requirements and procedures for physical testing. A class and grade are used to specify each type of well. The classes are A, B, C, D, G, and H. The grades are used to specify the level of sulfate resistance. Sulfate-resistant grades were developed to prevent deterioration of set cement downhole, caused by sulfate attack by formation waters. Well cements are available in either ordinary (O), moderate sulfate-resistant (MSR), or high sulfate-resistant (HSR) grades. Out of the classes, Class G and H are the most widely used. Both products are intended for use as basic well cement and are available in MRS and HSR grades.

2.2 Blended Cements

ASTM C 595 defines blended cement as a mixture of Portland cement and blast furnace slag or a mixture of Portland cement and a pozzolan (fly ash) [ASTM 2014]. The use of fly ash in cement and concrete provides numerous advantages. The small particle size of fly ash produces a smoother cement paste, allowing for better bonding between

aggregate and cement. This results in a more durable and impervious concrete [Zhang et al. 2011]. In addition to this, the hard and round shape of fly ash particles allow for an increase in concrete workability without adding extra water [Ahmaruzzaman 2010]. Other advantages of blending fly ash with cement include a reduction in pore size and in durability resulting from the hydration products of fly ash with calcium hydroxide ($Ca(OH)_2$), a positive effect on sulfate resistance, hydration heat, alkali-silicate reactions, and abrasion resistance [Atis 2002; Saraswathy et al. 2003; Yu et al. 2013].

2.3 Fly Ash

Fly ash is a byproduct of the coal industry, produced through the combustion of finely ground coal that is injected at high speeds into a furnace at electricity generating power plants. Once inside the boiler, the suspended coal is burnt instantaneously at temperatures around 1500 ˚C. The remaining matter present in the coal melts in suspension, cools rapidly as flue gases carry it out, and solidifies into fine spherical particles (typically 1 μm to 150 μm in diameter). Approximately 80% of the coal ash is carried out of the boiler by the flue gases and is removed before it is released into the atmosphere. The fly ash particles are usually extracted by means of electrostatic precipitators (Figure 2.1).

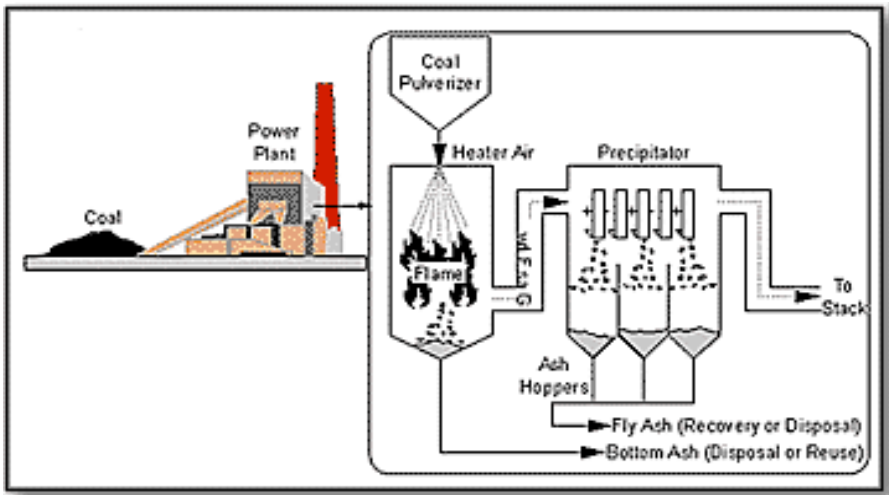

Figure 2.1 Process of fly ash production [Chesner 1998].

Fly ash can be divided into two classifications; ASTM Class F and ASTM Class C. This division is based on the chemical composition; more specifically, the calcium oxide (CaO) content. Class F fly ash is a low calcium fly ash that typically contains less than 10% CaO and is usually derived from anthracite and bituminous coals. Class C fly ash is a high calcium fly ash that contains greater than 10% CaO and is usually produced from subbituminous and lignite coals. The incombustible matter in the coal determines the composition of the fly ash. The chemical composition on fly ash is primarily composed of oxides of silicon (SiO_2), aluminum (Al_2O_3), iron (Fe_2O_3) and calcium (CaO) with lesser amounts of magnesium, potassium, sodium, titanium, and sulfur. The physical and chemical characteristics of fly ash depend on the combustion method, coal source, and particle shape. The chemical compositions present in different fly ashes demonstrate a wide range. This is believed to be due to wide variations in coal used in power plants all around the world [Malhotra et al. 1994]. Table 2.1 presents common ranges in chemical composition for the low calcium and high calcium fly ash [Davidovits 2008].

Table 2.1 Range of chemical composition for low and high-calcium fly ashes. [after Jarrige 1971].

Composition	Class F (%)	Class C Lignite based (%)
SiO_2	47.2 to 54	18 to 24.8
Al_2O_3	27.7 to 34.9	12.1 to 14.9
Fe_2O_3	3.6 to 11.5	6.3 to 7.8
CaO	1.3 to 4.1	13.9 to 49
Free lime content	0.1	18 to 25
MgO	1.4 to 2.5	1.9 to 2.8
SO_3	0.1 to 0.9	5.5 to 9.1
Na_2O	0.2 to 1.6	0.5 to 2
K_2O	0.7 to 5.7	1 to 3

The source and type of coal also affects the phase compositions of the fly ash spheres. The spheres are composed of amorphous (glass) and crystalline elements. The majority of the crystalline elements are mullite, haematite, magnetite, quartz, and unburned carbon residue. The chemical reactivity of the fly ash depends on the nature and proportion of glass phase present, which are partially dependent on the operating temperature at which the coal was burned.

The characteristics of fly ash that are generally considered in addition to chemical composition and glass phase are fineness, uniformity, and loss on ignition (LOI). The fineness of fly ash is dependent on the operating conditions of the coal crushers and the grinding process after cooling. Typically finer gradations result in more reactive ash and a reduced carbon composition. LOI is a measurement of the unburnt carbon that resides in the ash.

2.4 Geopolymers

A Polymer is a class of materials derived from large molecules that are composed of many repeating subunits (monomers). Polymers can be man-made or naturally occurring and have unique properties that can be modified for their intended purpose. The molecular structure of the monomers is what controls the properties of the material. A geopolymer is an example of an inorganic polymer.

The term geopolymer was first utilized by Professor Joseph Davidovits in 1979 [Davidovits 1979]. Davidovits originally described geopolymers as inorganic materials rich in silicon (Si) and aluminum (Al) that react with alkaline activators to become cementitious [Davidovits, 1991]. Geopolymer technology has a wide variety of potential applications; including fire resistant materials, thermal insulation, low-tech building materials, immobilization of toxic waste materials, etc. [Davidovits, 2008]. This is due to geopolymers exhibiting properties and characteristics such as high compressive strength, low shrinkage, fast or slow setting, acid resistance, fire resistance, and low thermal conductivity [Duxson et al. 2007]. The setting behavior, workability, and chemical and physical properties that make geopolymers suitable for different applications depend on the raw material used in geopolymer synthesis and the processing conditions [van Jaarsveld et al. 2003; Duxson et al. 2007].

The process of geopolymerization is one that involves the reaction of a solid aluminosilicate with a highly concentrated aqueous alkali hydroxide or silicate solution to produce a synthetic alkali aluminosilicate material [Davidovits, 1991]. Silico-aluminate based geopolymers are referred to as poly(sialates). The term sialate is an abbreviation for silicon-oxo-aluminate. The network of a sialate in amorphous phase consists of

tetrahedral silica (SiO_4) and alumina (AlO_4) linked alternately in 4-fold coordination by sharing all the oxygen atoms [Davidovits, 1976]. The general structure of poly(silates) is as follows:

$$M_n\{-(SiO_2)_z\text{-}AlO_2\}_n\, wH_2O \qquad (2\text{-}1)$$

where "z", the Si/Al ratio, is typically 1, 2, 3 or higher; M is a cation such as potassium or sodium, and "n" is a degree of polycondensation. The presence of positive ions (Na^+, K^+, Li^+, Ca^{++}, Ba^{++}, NH^{3+}, H_3O^+) in the three dimensional framework of the cavities is necessary to balance the negative charge of the Al^{3+} in IV-fold coordination [Davidovits, 1999].

Poly(sialates) are chain and ring polymers with Si^{4+} and Al^{3+} in IV-fold coordination with oxygen and range from amorphous to semi-crystalline. A geopolymer can take one of three basic forms for its structure depending on the Si/Al atomic ratio [Davidovits, 1999], i.e:

1. Poly(sialate) with [-Si-O-Al-O-] as the repeating unit (Si/Al = 1).
2. Poly(sialate-siloxo) with [-Si-O-Al-O-Si-O-] as the repeating unit (Si/Al = 2).
3. Poly(sialate-disiloxo) with [-Si-O-Al-O-Si-O-Si-O-] as the repeating unit (Si/Al = 3).

The formation of geopolymer material can be shown schematically by Equations (2-2) and (2-3) [van Jaarsveld et al. 1997; Davidovits 1999]. These formations indicate that any pozzolanic compound or source of silica and alumina that is readily dissolved in alkaline solution can be processed to make the geopolymer material.

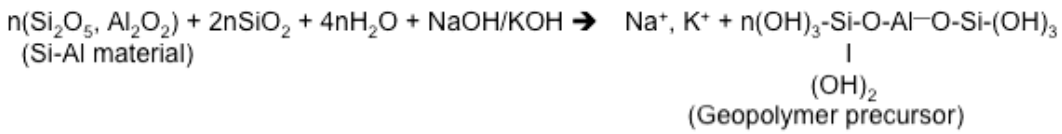

(2-2)

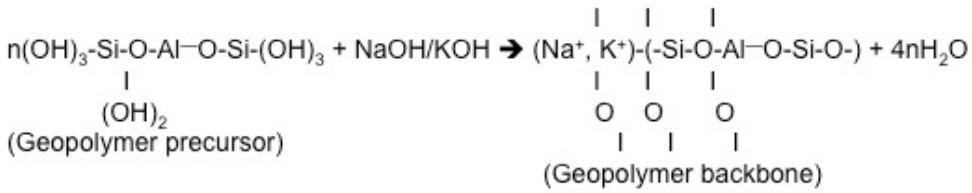

(2-3)

Presently, the exact mechanism of setting and hardening of a geopolymer is not fully understood. While many proposed mechanisms exist, the most popular is as follows [Davidovits 1999; Xu and van Deventer 2000; van Jaarsveld et al. 2002; Duxson et al. 2007]:

- Dissolution of the amorphous aluminosilicate source by alkali hydrolysis.
- Transportation, orientation or condensation of precursor ions into monomers.
- Setting or polycondensation of monomers into polymeric structures.

These steps can overlap and occur concurrently, thus making it difficult to isolate and study each step [Duson et al. 2007].

By further investigating the geopolymer design mixtures, Davidovits and his colleagues found that the molar ratio of Si to Al had a significant effect on material properties. A summary of these findings can be seen in Table 2.2. [Davidovits 1999].

Table 2.2 Applications of geopolymer materials.

Si/Al	Application
1	Bricks, ceramics, fire protection
2	Low CO_2 cements, concrete, radioactive & toxic waste
3	Heat resistance composites, foundry equipments fiber glass composites
>3	Sealants for industry
2-<Si/Al<35	Fire resistance and heat resistance fiber composites

2.4.1 Components of Geopolymers

2.4.1.1 Source Materials

Any raw material that is rich in silicon (Si) and Aluminum (Al) in amorphous form can be utilized as a potential source material for the production of a geopolymer. Past investigations have been carried out on utilizing industrial by-products and minerals as aluminosilicate source materials for geopolymer synthesis. Examples of investigated source materials are pozzolana [Allahverti et al. 2008; Verdolotti et al. 2008], natural aluminosilicate minerals [Xu and Deventer 1999], metakaolin or calcined kaolin [Davidovits 1991; Davidovits 1999; Duxson et al. 2007b, He et al. 2012], ASTM Class F and Class C fly ash [Palomo et al. 1999; Swanepoel et al. 2002; Gao et al. 2010; Guo et al. 2010], ground granulated blast furnace slag [Cheng and Chiu 2003], a combination of metakaolin and red mud [Zhang et al. 2010; He et al. 2012], and a combination of fly ash and metakaolin [Swanepoel et al. 2002; van Jaarsveld et al. 2002].

Much of the early research into geopolymer materials focused on utilizing metakaolin as the source material. Metakaolin is a calcined form of kaolinite, one of the earth's most abundant aluminosilicate clay minerals. The calcination of kaolinite takes

place at approximately 550-750 ˚C. Both the temperature and calcination time of kaolinite affect the ultimate surface area, degree of dehydroxylation, and reactivity of metakaolin. The base structure of metakaolin is that of a highly disrupted phyllosilicate structure, containing only silicon and aluminum. The particle size of metakaolin varies, but is generally smaller than 5 μm, with the fundamental size of clay being on the order of 20 nm [Duxson et al. 2007]. Davidovits (1999) studied the use metakaolin as a source material for geopolymers and suggested that for the purpose of making geopolymer cement, the molar ratio of Si to Al of the material should be around 2.0 (Table 2.2). Overall, studies have demonstrated that geopolymers formed from metakaolin can rapidly develop high strength and good thermal resistance [Davidovits 1991; Duxson et al. 2007; Duxson et al. 2007b; He et al. 2012]. Disadvantages associated with metakaolin-derived geopolymers are that they require an unreasonably high amount of water and display high porosity in concrete applications. This is thought to be due to metakaolin having a plate-like particle shape with a high surface area per unit volume. Because of these drawbacks geopolymer researchers began to investigate industrial wastes and other aluminosilicate materials as potential source materials.

Fly ash, unlike metakaolin, possesses a spherical particle shape. This results in lower water demand and a lower porosity attributed to maximized particle packing due to the particle shape [Duxson et al. 2008]. The majority of existing research focuses low-calcium (Class F) fly ash as a precursor for geopolymer material. This is primarily due to it being more widely available. However, a drawback to the Class F fly ash-based geopolymer is that it requires elevated temperatures for curing, thus challenging wide spread application. In an attempt to resolve this issue, researchers have looked into

increasing the fineness of the fly ash, to increase reactivity, and adding some calcium containing minerals [Li et al. 2007; Temuujin et al. 2009; Somna et al. 2011; Rashad et al. 2014]. It was found that the addition of high-calcium slag could greatly improve compressive strength of fly ash geopolymers at ambient temperatures. For this reason, it became common practice to incorporate ground granulated blast furnace slag with Class F fly ash in order to accelerate the initial hardening time of geopolymer slurries and to obtain higher strength.

A recent increase in use of lignite and sub-bituminous coals brought about a rise in geopolymer research focusing on high-calcium (Class C) fly ash as a source material. The publications focusing on the utility of Class C fly ash as a source material for geopolymers revealed that it is possible to utilize Class C fly ash in geopolymers and it would be preferable to Class F fly ash if the rheology of the mix can be adequately controlled [Roy et al. 1996; Lukey et el. 2006]. Compositionally, Class C fly ash can be viewed as resting somewhere between Class F fly ash and ground granulated blast furnace slag [Duxson et al. 2008]. This means that rather than combining the ground granulated blast furnace slag with Class F fly ash, Class C could potentially act as a single source material while providing all the benefits of early compressive strength at ambient temperatures.

While there are many benefits in utilizing fly ash as a source for geopolymer cement, the variation in elemental and phase composition of different fly ashes makes it difficult to determine an optimal mix design for a consistent product. As a result, research into the variation of fly ash and its impact on geopolymer products has been carried out and is still ongoing. Fernández-Jiménez and Palomo (2003) published a study on the

suitability of various types of low-calcium fly ash as source materials for geopolymers. The low-calcium fly ashes investigated were from Spain. Results of the study indicated that in order to produce optimal binding properties, the low-calcium fly ash required a percentage of unburned material (LOI) less than 5%, Fe_2O_3 content no higher than 10%, a low CaO content, a content of reactive silica between 40-50% and between 80 and 90% of its particle size lower than 45 μm in diameter. Contrary to this, van Jaarsveld et al (2003) published findings that fly ash with higher CaO produced higher compressive strength in geopolymers. This increase in strength with CaO content was attributed to the formation of calcium aluminate hydrate and other calcium compounds. In addition to chemical composition the particle size, amorphous content, morphology and origin are also characteristics that influence the suitability of fly ash as a source material for geopolymers.

2.4.1.2 Alkaline Activators

The type of alkaline activator used in geopolymerization plays an important role in the polymerization process (Palomo et al. 1999). The most common alkaline activators utilized in geopolymer research are a combination of sodium hydroxide (NaOH) or potassium hydroxide (KOH) and sodium silicate or potassium silicate [Davidovits 1999; Palomo et al. 1999; Xu and van Deventer 1999; Swanepoel et al. 2002]. Out of these activators, sodium hydroxide (NaOH) and sodium silicate are most commonly used due to cost and availability [Turner, 2013].

Palomo et al. (1999) investigated the mechanism of activation of fly ash with different alkaline activators. As a result, he found that alkali activators containing soluble silicates (sodium or potassium silicate) produced higher reaction rates compared to those only containing hydroxides. Xu and van Deventer (1999) confirmed these findings during their study of sixteen natural Al-Si minerals. In addition to this, they found that the activator solution containing NaOH typically resulted in a higher extent of dissolution of minerals than the KOH solution.

2.4.2 Mixture Proportions

Raw materials play an essential role in the geopolymerization reaction and control the chemical reaction and microstructure of the final geopolymer product. Much of the existing research into geopolymers primarily focuses on the effect of design mixture on the curing and mechanical properties of geopolymers. Past investigations into geopolymers has considered the effect the molar ratio of SiO_2/Na_2O, SiO_2/Al_2O_3, and H_2O/Na_2O on specific properties for cement.

In 2012, He et al. investigated the effect of source materials on the microstructure and mechanical properties of two types of geopolymer synthesized from metakaolin and an admixture of red mud and fly ash [He et al. 2012]. In order to explore the influence of Si/Al ratio on compressive strength, the metakaolin-derived geopolymer specimens were prepared at three different Si/Al ratios of 1.25, 1.75, and 2.25, while the Na_2O/SiO_2 and H_2O/Na_2O molar ratios remained constant at 0.3 and 17.5, respectively. The effect of Si/Al on curing duration was investigated for the specimens possessing a Si/Al ratio of

1.75. The five different curing durations selected were 5, 9, 14, 21, and 28 days. Each geopolymer specimen was prepared to be 2 cm in diameter and 5 cm in height to create an aspect ratio of 2.5 and minimize the end effects. Overall, it was found that the compressive strength of the geopolymers studied increased with curing duration and Si/Al ratio and reached a constant after complete curing had occurred. The metakaolin geopolymer with the largest Si/Al ratio achieved strength of approximately 31 MPa.

Guo et al. (2010) investigated the compressive strength and microstructural characteristics of Class C fly ash geopolymers. The geopolymers, in this study, were prepared using Class C fly ash and a mixed alkali activator solution of sodium hydroxide and sodium silicate solution. The modulus of the mixed alkali activator was investigated at SiO_2/Na_2O molar ratios of 1.0, 1.5, and 2.0. Each specimen was prepared with a mass ratio of water to Class C fly ash of 0.4.and the mixed activator was evaluated by the mass proportion of Na_2O to Class C fly ash. Each geopolymer specimen was prepared and poured into 20 mm x 20 mm x 20 mm cubic molds. The effects of curing conditions were investigated through the variation of curing temperature and duration. One batch of specimens were placed immediately in an air-conditioned room at 23 ˚C and cured for durations of 3, 7, and 28 days. The other batch was first cured in an oven at elevated temperatures of 60-90 ˚C for 4, 8, and 24 hours and then followed the same curing duration and condition as the first batch. Overall, it was found that compressive strength increased with curing duration and Na_2O concentration. The highest compressive strength for both batches was exhibited in the specimens that possessed a modulus of activator of 1.5 M and a content of activator of 10%. The geopolymers cured immediately at 23 ˚C, displayed a peak compressive strength of 59.3 MPa after 28 days of curing. The

geopolymers cured at the 75 ˚C for 8 hours followed by curing at 23 ˚C for 28 days, displayed a peak compressive strength of 63.4 MPa.

2.4.3 Factors Affecting Properties of Geopolymers

Several factors affect the properties of geopolymers. Palomo et al. (1999) concluded that curing temperature increased the reaction of fly ash-based geopolymers and had a significant effect on the mechanical strength, in addition to curing time and the type of alkaline activator used. Higher compressive strength was observed in specimens cured at elevated temperatures with longer curing times. The study by Guo et al. (2010) supported the conclusion that higher curing temperature and curing duration results in higher compressive strength.

Based on a study of metakaolin-based geopolymers, He et al. (2012) concluded that the compressive strength increased with both curing duration and the molar ratio of Si/Al. Chindaprasirt et al. (2012) reported that the ratio of SiO_2/Al_2O_3 affected the setting and hardening of high calcium fly ash-based geopolymers. It was found that an increase in either silica or alumina accelerated setting time with an optimal SiO_2/Al_2O_3 ratio in the range of 3.20-3.70. However, further increase in silica (SiO_2/Al_2O_3 >4) resulted in a decrease in strength.

In studying the effect of composition and temperature on the properties of fly ash-based and kaolinite-based geopolymers, van Jaarsveld et al. (2002) concluded that water content, curing as well as calcination conditions influence the final properties of geopolymers. However, rapid curing and/or curing at high temperatures resulted in

cracking and a negative effect on the physical properties of the kaolin-based geopolymers.

3 EXPERIMENTAL PROGRAM

3.0 Introduction

This chapter primarily focuses on the details of the materials used in this research, the development process of making the Class C fly ash/metakaolin-based geopolymer cement, the process of designing a curing environment, and the finalized process of preparation and curing of the cement cylinders. The present study utilized published papers as a source of reference to synthesizing geopolymers from metakaolin and Class C fly ash. Research related to simulating saline water environments was also utilized.

3.1 Materials

The raw materials used to synthesize the geopolymer cement were Class C fly ash (Headwater Resources, MA, USA), PowerPozz TM metakaolin (Advanced Cement Technologies, LLC, USA), sodium silicate solution consisting of 28.7 wt. % SiO_2, 8.9 wt. % Na_2O and 62.7 wt. % H_2O (Fisher Scientific of Thermo Fischer Scientific Inc., USA), and sodium hydroxide pellets (>95% purity quotient, Fisher Scientific of Thermo Fisher Scientific Inc., USA). For benchmarking purposes, Class G well cement (Lafarge, USA) was also used for strength testing. The chemical compositions of the fly ash, metakaolin and Class G cement used in this research, as determined by X-ray fluorescence (XRF) analysis, are presented in Table 3.1. The XRF analysis was carried out by the Geosciences Department, University of Massachusetts, Amherst, MA and details of this analysis are presented later on in Section 4.2 of Chapter 4.

Table 3.1 Composition of Fly Ash, Metakaolin and Class G Cement as Determined by XRF (mass %).

Oxides	Class C Fly Ash	Metakaolin	Class G Cement
SiO_2	37.93	53.80	17.75
Al_2O_3	19.99	40.11	3.21
Fe_2O_3	6.78	2.00	4.18
CaO	22.55	0.04	63.61
Na_2O	1.60	0.02	0.004
K_2O	0.52	0.29	0.19
TiO_2	1.45	1.39	0.20
MnO	0.04	0.003	0.10
MgO	5.01	0.08	0.93
P_2O_5	1.23	0.16	0.02

3.1.1 Grain Size Distribution of Source Materials

Grain size analyses were performed on samples of fly ash and metakaolin. For each analysis, a nominal 55 to 60 grams of each raw material was tested in general accordance with ASTM D442-90: Standard Test Method for Particle-Size Analysis of Soils [ASTM 2011]. A visual inspection indicated that both samples tested were comprised almost entirely of fines (<#200 sieve). For this reason, a 152H hydrometer was utilized to determine the grain size for each sample.

First, approximately 60 grams of each sample was weighed, thoroughly mixed with 125 ml of sodium hexametaphosphate solution (40 g/L) and allowed to soak overnight (a minimum of 16 hours). Sodium hexametaphosphate is a dispersing agent that can break down soil to its smallest particles. After the required soaking period, hydrometer tests were conducted in a temperature control box using a 152H hydrometer

and a control cylinder. Hydrometer readings were recorded at the following intervals of time: 1, 2, 4, 8, 15, 30, 60, 240, 480, and 1440 min. At the end of the 1440-minute (24 hour) test, the sample solution was passed through a #200 sieve. Sample particles passing the #200 sieve were collected, oven dried and weighed to support the particle distribution results. Sample particles retained on the #200 sieve were also collected, oven dried and weighed. The resulting particle size distribution of the fly ash and metakaolin are presented in Figure 3.1 and Figure 3.2, respectively.

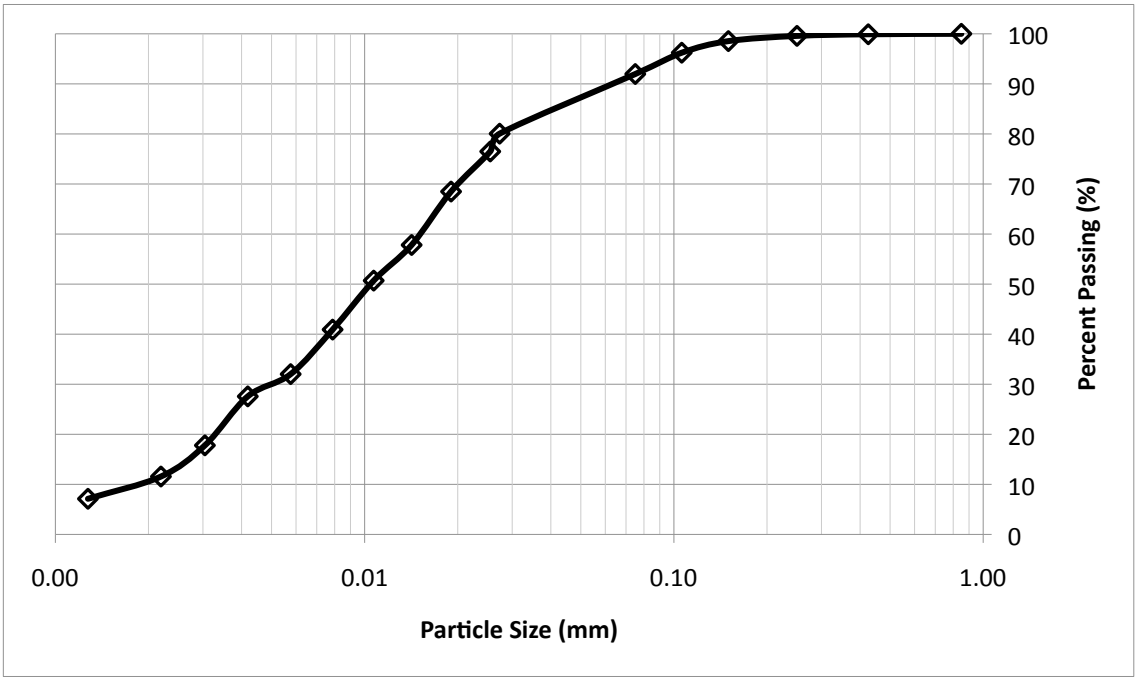

Figure 3.1 Particle size distribution for Class C fly ash.

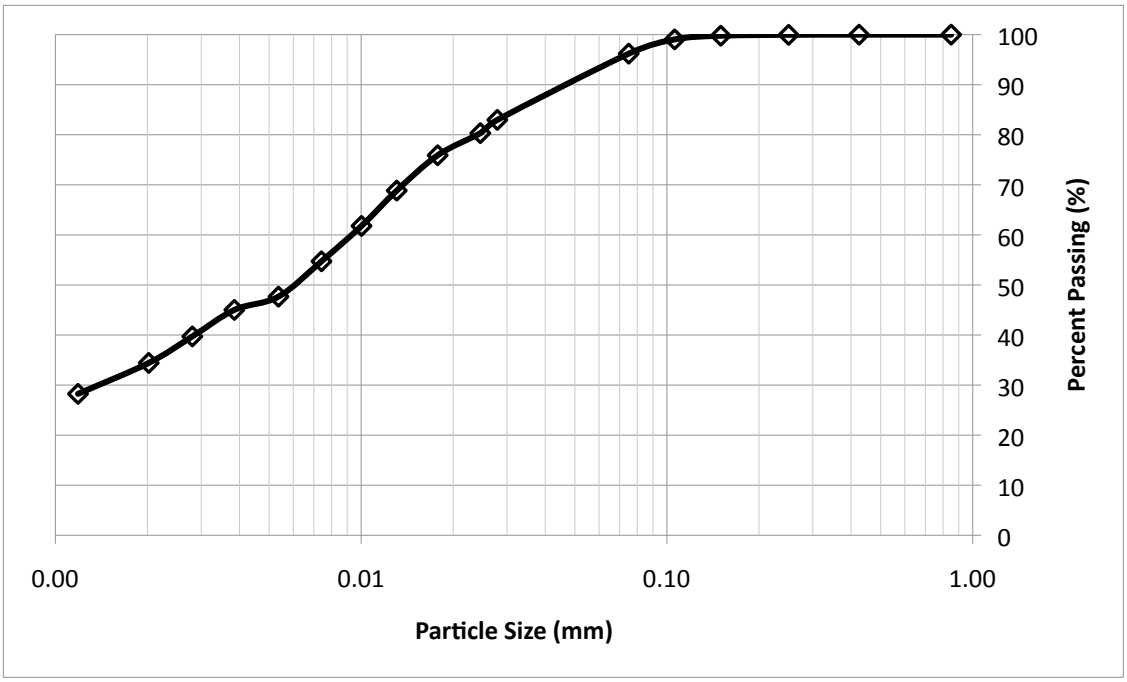

Figure 3.2 Particle size distribution for metakaolin.

Both the Class C fly ash and metakaolin were predominantly composed of silt-sized particles. The compositional breakdown of particle size can be seen in Table 3.2.

Table 3.2 Summary of material components.

Component	Class C Fly Ash	Metakaolin
% Sand	8.0	3.8
% Silt	81.3	61.9
% Clay	10.6	34.3

3.2 Preliminary Laboratory Work

The preliminary laboratory work for the present study involved designing various trial mix designs, developing a method of preparation and curing for trial mix specimens, specimen testing and selection of finalized a design mix for the investigation.

3.2.1 Development of Trial Mixes

At the beginning of this research, numerous mixtures of geopolymer cement were developed and test specimens were prepared as cylinders with a diameter of 2 cm and a height of 5 cm. The cylinder dimensions were selected to provide an aspect ratio of 2.5 and to minimize end effects.

The primary objectives of the preliminary laboratory work were as follows:

- To become familiar with the process of making metakaolin and fly ash-based geopolymer cement.
- To understand the effect of sequence on preparing the activator solution and adding it to the solid constituents.
- To observe the behavior and workability of the geopolymer cement.
- To develop of method of mixing and curing.
- To understand the effect of mixture proportion on behavior and workability of geopolymer cement.

The first stage of developing trial design mixes required selecting reference mixes from published papers on the utilization of metakaolin and Class C fly ash as precursors for geopolymer cement. The study by He et al. (2012) was the source of reference for the metakaolin mix. As mentioned in Section 2.4.2, this investigation focused on the strength and microstructure of two geopolymers, one derived from metakaolin and the other from a red mud-fly ash admixture. The highest compressive strength for the metakaolin-derived geopolymer cement occurred at 31 MPa after 28 days of curing at ambient temperatures. The mix that produced this value possessed the following molar ratios: Si/Al = 2.25, Na_2O/SiO_2 = 0.3, and H_2O/Na_2O = 17.5.

The study by Guo et al. (2010) was the source of reference for the Class C fly ash mix. As mentioned in Section 2.4.2, this investigation studied the effect of curing duration, curing condition, and modulus of activator (molar ratio of SiO_2/Na_2O). The highest compressive strength for the Class C fly ash-derived geopolymer cement occurred at 59.3 MPa after 28 days of curing at ambient temperatures. This mix possessed a modulus of activator = 1.5 M, a mass content of Na_2O in the activator to fly ash of 10%, and a mass ratio of H_2O to fly ash of 0.40.

Table 3.3 presents the different design mixes that developed from the selected references. When developing the trial mixes, the reference mixes were first replicated and then altered depending on the behavior during preparation and final cured product. MK-A was the trial mix that replicated the metakaolin reference. This mix was observed to be overly watery when mixing and produced a cured product that was low in strength and crumbled in certain areas. The MK-B mix was an alteration on the original metakaolin mix where the water content was reduced by 50%. This mix produced a more desirable consistency and cured product. Flash setting was experience while attempting to recreate the Class C fly ash reference mix. Flash setting is when the rate of reaction was too fast and the mixture hardened during mixing. In an attempt to reduce the rate of reaction, a new mix was created (CFA-A) where additional water was added and the content of sodium hydroxide was reduced by 50% to lower the pH. While the workability and rate of reaction were both improved, the final cured product presented fine horizontal cracking. In order to eliminate the cracking, half of the mass of fly ash was replaced with metakaolin in the CFA-A mix (CFA/MK-A). This resolved the horizontal cracking and produced a final product that was un-fissured.

Table 3.3 Summary of trial geopolymer cement mixtures and their design components.

Trial Mix Name	Mixed Alkali Activator	Geopolymer Slurry				
	SiO_2/Na_2O	Si/Al	Na/Si	$Na_2O_{activator}$/Raw Material (wt. %)	$H_2O/Na_2O_{activator}$	H_2O/Raw Material (wt. %)
MK-A	1.52	2.25	0.6	32.15	17.5	164
MK-B	1.52	2.25	0.6	32.15	14.25	133
CFA-A	2.07	2.28	0.32	7.27	22.9	48
CFA/MK-A	2.07	1.78	0.25	7.27	22.8	48

3.2.2 Specimen Preparation

For the synthesis of the trial geopolymer cements, sodium hydroxide (NaOH) was first dissolved into reverse osmosis (RO) water and allowed to cool. Once cooled the solution was mixed with sodium silicate for a minimum of 5 minutes, covered, and allowed to rest overnight. The next day the selected powdered raw material was added to the prepared activator solution and hand mixed for a minimum of 15 minutes to ensure complete mixing between the powder and the solution. The mixed product resulted in a geopolymer precursor in the form of slurry.

3.2.3 Specimen Casting and Curing

Each trial specimen was cured in dry conditions within a plastic split mold that possessed an inner diameter of 2 cm and a height of 5 cm (Figure 3.3 Components of split molds used for trial specimen curingFigure 3.3). Prior to assembling, the interior of the mold was coated with a thin layer of vacuum grease to allow for easy removal of the cement specimen after the 28 day curing duration. An Everbit stainless steel clamp was

utilized to keep the split mold together and create a tight seal along the seams of the mold.

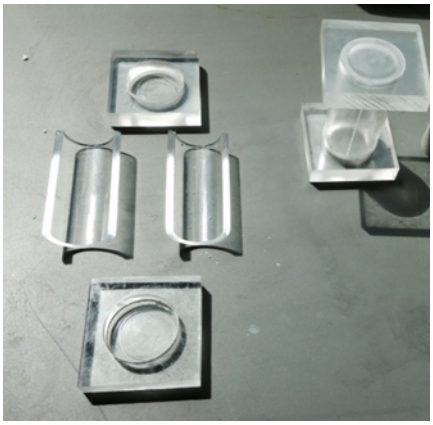

Figure 3.3 Components of split molds used for trial specimen curing.

Once each mold had been prepared and assembled, the geopolymer cement slurry was mixed and poured into each mold, vibrated (tapped) by hand for air removal, covered, and allowed to cure for a 28 day duration (Figure 3.4).

Figure 3.4 Cured trial specimens prior to de-molding.

3.2.4 Specimen Testing

After the 28 day curing duration, each trial specimen was de-molded (Figure 3.5 and Figure 3.6). Compression tests were performed on each cylinder to determine which

cured mix produced the highest unconfined compressive strength. All tests were performed at the Geotechnical Engineering Laboratory, University of Massachusetts Amherst, in general accordance with ASTM C39/C39M-14: Standard Test Method for Compressive Strength of Cylindrical Concrete Specimens [ASTM 2014].

Figure 3.5 Grouped de-molded trial cylinders.

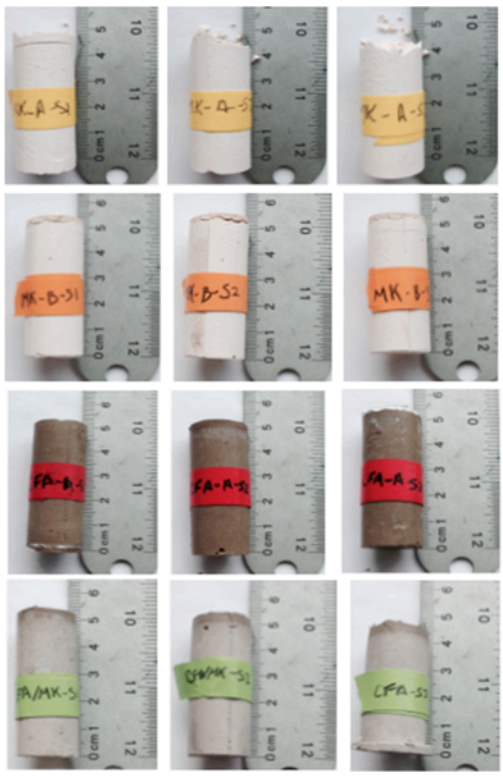

Figure 3.6 Individual de-molded trial cylinders.

Prior to testing, the end of each test specimen was made level by sanding to meet the perpendicularity requirements of the standard. In addition to this, the diameters and heights of each specimen were recorded and the cross sectional area was determined to the nearest 0.25 mm. Once level, a thin layer of vacuum greased was applied to the cylinder ends to eliminate friction during testing.

Compression tests were performed using a GEOTAC 10,000 lb. Load Frame equipped with an automated data acquisition system. Each test was strain controlled with a strain rate of 15% deformation per minute.

The results of the compression testing revealed that the CFA/MK-A mix achieved the highest compressive strength at 29.25 MPa (Figure 3.7). This mix was selected for the

final design due to its excellent workability, rate of reaction, observed cured condition, and high compressive strength.

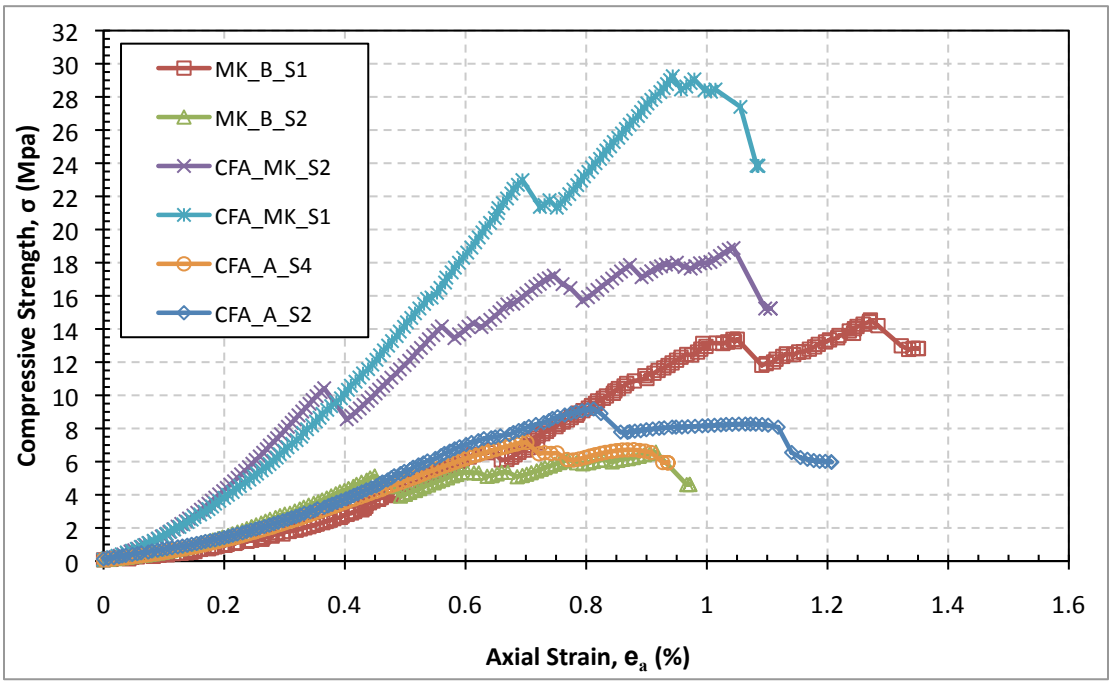

Figure 3.7 Plot of unconfined compressive strength versus percent strain for trial cylinders.

3.3 Experimental Design

3.3.1 Cement Mold

In order to design an adequate mold for casting and curing of the cement cylinders, certain requirements had to be met. These requirements were as follows:

- To be reusable, fully encase cement specimen and allow for easy removal of cement after complete curing.
- To be resistant to acidic environments.
- To allow for saline water and cement interaction.

- To have the ability to retain fly ash particles during immediate curing in saline water environment.

In order for the mold to be reusable, fully encase the cement specimen, and allow for easy removal, a split mold design with end caps was selected (Figure 3.8). The split mold was designed to be 1.5 in. in diameter and 3.5 in. in height. This provided an aspect ratio of 2.3 and minimized end effects.

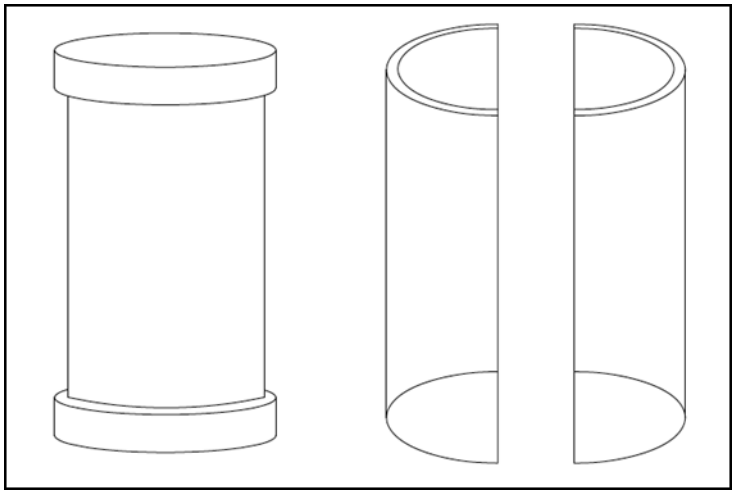

Figure 3.8 Schematic of split mold with end caps for cement casting and curing.

Each split mold was cut from polyethylene permeable tube (obtained from Permaplas Corporation). This tube possessed a pore size of 10 μm, which allowed for saline water and cement interaction. The end caps were fabricated from natural polyvinylidene fluoride (obtained from Emco Industries Plastics, Inc.). Both the polyethylene tube and end cap material were chosen for their excellent chemical resistance properties. The split molds and end caps were machined at the Smith College Center for Fabrication and Design (Figure 3.9). An inner filter made of Grade 410 filter paper was incorporated into the design to ensure fly ash particle retention. This filter paper had ability to retain particles 1 μm in diameter and was cut to fit the inner

circumference of the split mold. Once assembled, the split mold was held together using an Everbit stainless steel clamp (Figure 3.10).

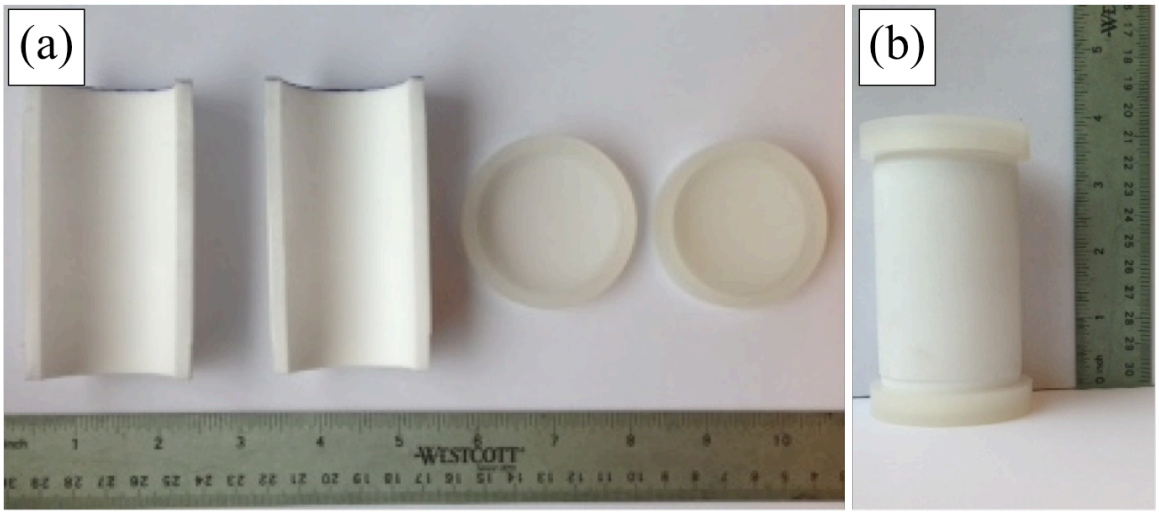

Figure 3.9 Fabricated split mold, (a) machined split mold and end caps, (b) front view of assembled split mold.

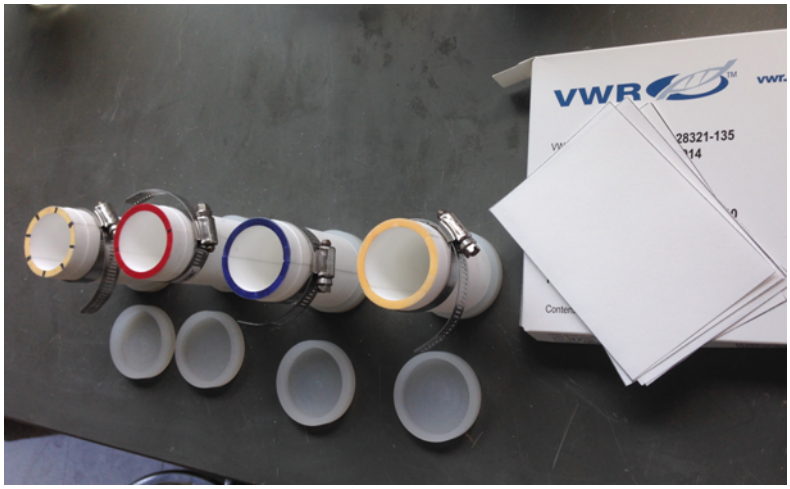

Figure 3.10 Assembled split molds with pre-cut inner filters.

3.3.2 Curing Environment

Three main requirements were considered while designing the curing environment. The requirements for the curing environment were as follows:

1 To simulate offshore environment.

2 To provide isolated curing for each specimen.

3 To provide a consistent saline curing environment for each specimen cured at a desired salinity.

In order to simulate an offshore environment, methods of developing saline water had to be considered. Giasuddin et al. (2013) investigated the strength of a Class F fly ash-derived geopolymer cured in saline water at ambient conditions. In this study the geopolymer cement was prepared using an admixture of the fly ash and a small percentage of ground granulated slag. Once prepared and cast, the cement slurry was cured in within the mold for 10-12 hrs, de-molded, and placed in curing waters for the 28 day water curing duration. The saline water was prepared by adding sodium chloride (NaCl) to water at different concentrations. Using chemicals such as NaCl is a common method of preparing saline water at different concentrations in research.

For the present research, it was desirable to attempt a less common route of developing saline water. This lead to an investigation of the viability of commercial sea salts for the simulation of offshore environments. Atkinson and Bingman (1997) investigated the elemental composition of commercial sea salts. In this study, the composition of eight synthetic saltwater mixes were compared to ocean water. Thirty-five grams of each salt sample was mixed into highly purified water and brought to one liter. The objective of this method of sample preparation was to simulate the salinity of ocean

water, approximately 35 parts per thousand (ppt). Each sample was analyzed for salinity, the major cations and anions, nutrient compounds and trace elements. It was determined that Instant Ocean Aquarium Sea Salt was compositionally the closest to ocean water. For this reason, Instant Ocean Aquarium Sea Salt was selected to simulate saline water environments immediate curing of the cement specimens.

An isolated curing environment was created for each specimen using a 700 mL glass beaker. The beaker would facilitate isolating curing by encasing each specimen in curing water. To ensure consistent saline curing environments for each specimen cured, the curing water would be batch mixed to the desired salinity and partitioned into the different beakers.

3.3.3 Specimen Preparation and Curing

The CFA/MK-A cement slurry was prepared using the procedure used for the trial cylinders. However, it should be specified that the powdered Class C fly ash and metakaolin were fully blended prior to mixing with the alkaline activator solution. After the 15 minutes of mixing the geopolymer cement slurry was poured into the preassembled porous split molds, leveled off, and vibrated (tapped) by hand to remove trapped air (Figure 3.11). Once trapped air had been removed, the top cap was secured on the mold and the specimen was placed into the empty 700 mL beaker. Next, the previously batch-mixed curing water was poured over each sample until full submersion was achieved. Once adequately filled, each beaker was covered with parafilm and plastic

wrap, placed out of direct sunlight, and allowed to sit for the 28 day curing duration (Figure 3.12).

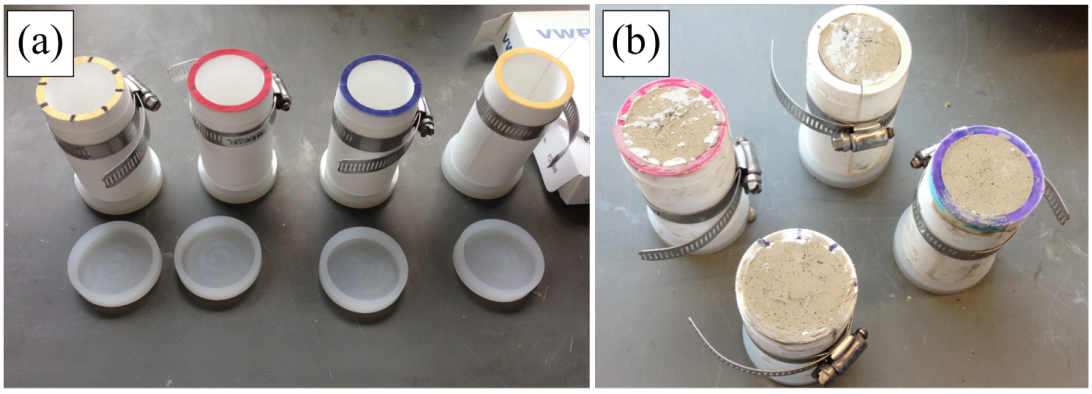

Figure 3.11 Specimen casting: (a) preassembled split molds for cement casting; (b) split molds filled with cast cement.

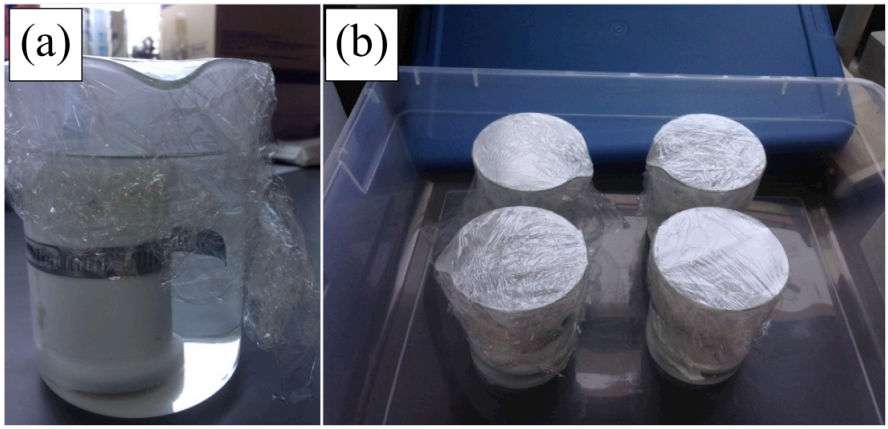

Figure 3.12 Specimen curing: (a) immediate water curing of isolated specimens; (b) specimen storage during curing.

The Class G cement, obtained from Lafarge, was produced using recommended cement to water ratio of 0.44 (value provided by Lafarge). RO water was added to dry Class G cement and mixed for 15 minutes to ensure complete mixing. The procedure of specimen casting and curing that was followed for the CFA/MK-A geopolymer cement was also applied for the Class G cement for comparability. Table 3.4 provides a summary of the specimens created for this investigation and their curing durations.

Table 3.4 Summary of cement specimens.

Specimen Name		Days Curing	Cure Start Date	Cure End Date
CFA/MK-A	35ppt-S1	28	Friday, September 12, 2014	Friday, October 10, 2014
	35ppt-S2	28	Friday, September 12, 2014	Friday, October 10, 2014
	35ppt-S3	28	Friday, September 12, 2014	Friday, October 10, 2014
	35ppt-S4	28	Friday, September 12, 2014	Friday, October 10, 2014
	35ppt-S5	28	Wednesday, January 07, 2015	Wednesday, February 04, 2015
	15ppt-S1	28	Thursday, October 16, 2014	Thursday, November 13, 2014
	15ppt-S2	28	Thursday, October 16, 2014	Thursday, November 13, 2014
	15ppt-S3	28	Thursday, October 16, 2014	Thursday, November 13, 2014
	15ppt-S4	28	Thursday, October 16, 2014	Thursday, November 13, 2014
	15ppt-S5	28	Wednesday, January 07, 2015	Wednesday, February 04, 2015
	0ppt-S1	28	Tuesday, November 18, 2014	Tuesday, December 16, 2014
	0ppt-S2	28	Tuesday, November 18, 2014	Tuesday, December 16, 2014
	0ppt-S3	28	Tuesday, November 18, 2014	Tuesday, December 16, 2014
	0ppt-S4	28	Tuesday, November 18, 2014	Tuesday, December 16, 2014
GC	35ppt-S1	28	Friday, September 12, 2014	Friday, October 10, 2014
	35ppt-S2	28	Friday, September 12, 2014	Friday, October 10, 2014
	35ppt-S3	28	Friday, September 12, 2014	Friday, October 10, 2014
	35ppt-S4	28	Wednesday, January 07, 2015	Wednesday, February 04, 2015
	15ppt-S1	28	Thursday, October 16, 2014	Thursday, November 13, 2014
	15ppt-S2	28	Thursday, October 16, 2014	Thursday, November 13, 2014
	15ppt-S3	28	Thursday, October 16, 2014	Thursday, November 13, 2014
	15ppt-S4	28	Wednesday, January 07, 2015	Wednesday, February 04, 2015
	0ppt-S1	28	Tuesday, November 18, 2014	Tuesday, December 16, 2014
	0ppt-S2	28	Tuesday, November 18, 2014	Tuesday, December 16, 2014
	0ppt-S3	28	Tuesday, November 18, 2014	Tuesday, December 16, 2014

4 CHARACTERIZATION OF STRENGTH

4.0 Introduction

The characterization of strength of the hardened Class C fly ash/metakaolin-based geopolymer cement and Class G cement was accomplished through strength testing and testing of other properties influencing strength. The following sections provide details into the materials and methods, the results of testing, and a discussion of the results.

4.1 Materials and Methods

4.1.1 Testing Materials

In order to obtain and understand the strength properties of the cement specimens, the 28-day cured geopolymer and Class G cement specimens were used in the laboratory tests described in this section. The cement specimens were inspected for flaws that might negatively impact the validity of results. Any specimens containing significant flaws was to be discarded and not used for further testing.

4.1.2 Moisture Content

Cement specimen moisture contents were measured for each specimen prior to strength testing. Moisture contents were determined in general accordance with ASTM Standard D2216-10: Standard Test Method for Laboratory Determination of Water (Moisture) Content of Soil and Rock [ASTM 2011].

Moisture Content is a property that can be used to predict and explain strength characteristics of cement. Typically the moisture content, or water absorbed into cement, is an indication of porosity and can impact strength. After the 28 days of water curing, each specimen was de-molded and immediately weighed to obtain a wet mass. Each specimen was then allowed to air dry for a minimum of two weeks. The specimens were weighed periodically during this drying period. Once negligible change was observed in weight measurements, the sample was considered dry and the final weight was recorded as the dry weight. The wet weight and dry weight of the cement was then used to obtain the moisture content using the following equation.

$$w = \frac{W_{wet} - W_{dry}}{W_{dry}} \times 100\% \tag{4-1}$$

where

w = water content (%)

W_{wet} = wet weight of cement specimen (g)

W_{dry} = dry weight of cement specimen (g)

4.1.3 Bulk Density

Cement specimen bulk densities were measured for each specimen prior to strength testing. Typically, density has a positive correlation to the strength and therefore could be used to support results from strength testing. The dry weight and volume of each cylindrical specimen was used to obtain the bulk density using Equation 4-2.

$$\rho = \frac{W_{dry}}{V_T} \tag{4-2}$$

where

ρ = bulk density (g/cm^3)

W_{dry} = dry weight of cement specimen (g)

V_T = total volume of cement specimen (cm^3)

4.1.4 Compressive Strength Tests

Compressive strength tests were performed in accordance to ASTM C39/C39M: Standard Test Method for Compressive Strength of Cylindrical Concrete Specimens [ASTM 2001]. All tests were performed in the Piece Laboratory at Massachusetts Institute of Technology (MIT). A MTS 100,000 lb. test machine equipped with a 100,000 lb. load cell was utilized for each test. An Instron 8500 Plus, retrofitted to the test machine frame, was used as the controller during testing. The following sections provide the details of sample preparation and testing.

4.1.4.1 Sample Preparation

ASTM C39/C39M-14 requires the end of compression test specimens to be plane within 0.50 mm (0.002 in.). Any sample that deviates from the planeness or perpendicularity requirements is required to sawed or ground to meet the tolerance, or capped in accordance with ASTM Standard C617: Practice for Capping Cylindrical Concrete Specimens [ASTM 2012]. To adhere to the perpendicularity requirement, each cylinder was sanded using coarse Grade 60 sand paper. However, early testing indicated that sanding alone did not ensure adequate perpendicularity of the surface. For this

reason, the practice of capping was followed. The hard plaster method of capping was selected for the purpose of this investigation.

The specifications for Practice C617 include requirements for the capping material and the method of capping. The Department of Civil Engineering at MIT followed this standard to machine a vertical capper and the capper was used to cap the specimens tested in this investigation (Figure 4.1). Plaster of Paris was the capping compound typically utilized by MIT for concrete cylinder capping, therefore that same compound was used to cap the cylinders for this investigation (Figure 4.2).

Figure 4.1 Vertical cylinder capper used to cap cylinders prior to strength testing.

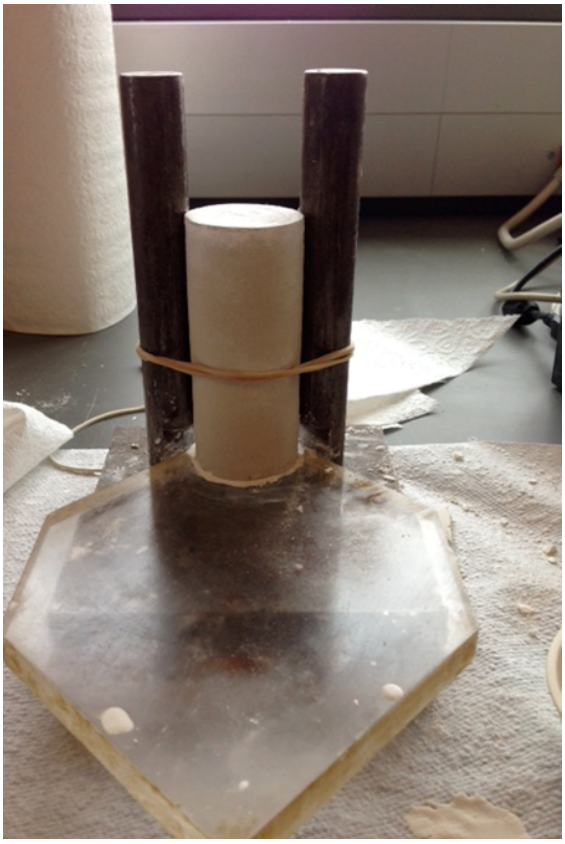

Figure 4.2 Vertical cylinder capper being used to cap a cement cylinder.

Prior to capping, the acrylic plate was lubricated with a thin layer of WD-40 to allow for easy removal of the cured plaster. The wet plaster used to cap each cylinder consisted of a plaster to water ratio of approximately 2:1. Once the wet plaster was mixed to the desired consistence, it was placed on the end of the cylinder. Next, cylinder was strapped against the alignment rods and the plastered end was pushed onto the plastic plate. Excess plaster was neatly removed and the cylinder was left in place for approximately 20 minutes to allow to adequate curing of the plaster. The capped cylinder was then removed and set aside for further curing. The cap was later sanded along the edges, using very fine Grade 220 sand paper, until it was flush with the sides of the cylinder. This process was repeated for the other end of the cylinder.

4.1.4.2 Compressive Strength Testing

As mentioned previously, all compression tests were performed using a MTS 100,000 lb. test machine equipped with a 100,000 lb. load cell (Figure 4.3). Prior to testing, each specimen was equipped with two extensometers to measure internal deformation. Once assembled and placed in the machine, stress controlled tests were carried out following a recommended stress rate of 0.25 ± 0.05 MPa/s [35 ± 7 psi/s]. Figure 4.4 presents an example to the test set up within the MTS test machine prior to load application. Each cylinder was tested until failure and collected afterward for further analysis (Figure 4.5). The data acquired from testing was processed and used to identify the peak compressive strength, failure strain, and Young's modulus for each cement specimen.

Figure 4.3 MTS 100,000 lb. test machine equipped with 100,000 lb. load cell.

Figure 4.4 Cement specimen prior to application of compressive load.

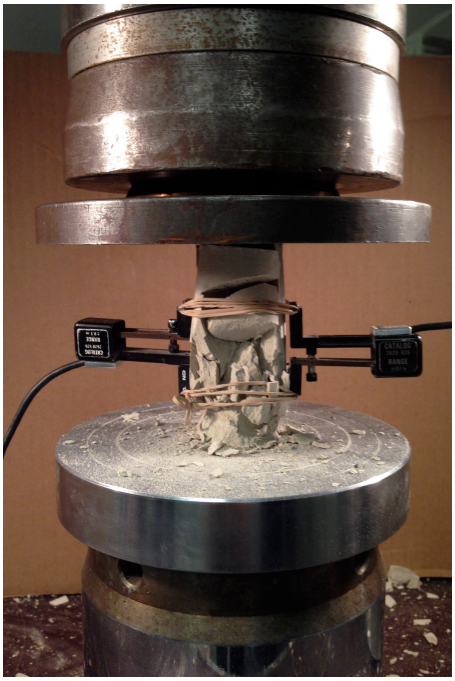

Figure 4.5 Cement specimen after reaching a state of failure during unconfined compression tests.

4.2 Results and Discussion

Table 4.1 presents a summary of the properties obtained for the cement specimens before and after carrying out unconfined compression tests. It can be observed from the table that the moisture content is generally decreasing with increasing salinity of curing environments. As expected, the bulk density increases with decreasing moisture content. Plots of compressive strength as a function of axial strain are presented for the geopolymer cements and Class G cements in Figures Figure 4.6 through Figure 4.8 and Figures Figure 4.9 through Figure 4.11, respectively. The axial strains plotted in these figures were calculated from an external measurement of the change in height, rather than from the internal, since the tests were stress controlled.

Table 4.1 Summary of properties for the cement specimens tested.

Specimen Name		Moisture Content [%]	Bulk Density [g/cm^3]	Peak Compressive Strength [MPa]	Failure Strain [%]	Young's Modulus [GPa]
CFA/MK-A	0ppt-S1	26	1.45	33.1	1.38	3.2
	0ppt-S2	27	1.44	27.0	1.08	3.0
	0ppt-S3	26	1.44	19.1	0.98	2.8
	0ppt-S4	26	1.42	34.4	1.17	3.7
	15ppt-S1	25	1.46	36.6	0.93	5.8
	15ppt-S2	25	1.49	34.9	0.98	5.1
	15ppt-S3	25	1.49	41.4	1.08	5.0
	15ppt-S4	25	1.49	41.8	1.06	5.8
	15ppt-S5	25	1.72	24.9	0.81	3.1
	35ppt-S1	24	1.59	24.2	0.71	4.3
	35ppt-S2	24	1.48	58.5	1.69	5.9
	35ppt-S3	23	1.50	32.5	0.91	4.6
	35ppt-S4	24	1.49	55.7	1.45	5.3
	35ppt-S5	25	1.82	35.4	1.31	3.0
GC	0ppt-S1	11	1.78	53.7	1.24	6.1
	0ppt-S2	12	1.78	62.9	1.30	7.7
	0ppt-S3	10	1.87	41.5	1.38	4.3
	15ppt-S1	7	1.95	31.8	0.64	6.7
	15ppt-S2	6	1.97	31.9	1.07	5.0
	15ppt-S3	7	1.99	59.0	0.75	10.3
	15ppt-S4	6	1.69	38.5	0.92	5.8
	35ppt-S1	8	1.99	44.0	1.13	7.3
	35ppt-S2	8	1.91	23.1	1.00	4.3
	35ppt-S3	8	1.97	33.7	1.00	4.3
	35ppt-S4	5	1.84	35.9	1.28	3.8

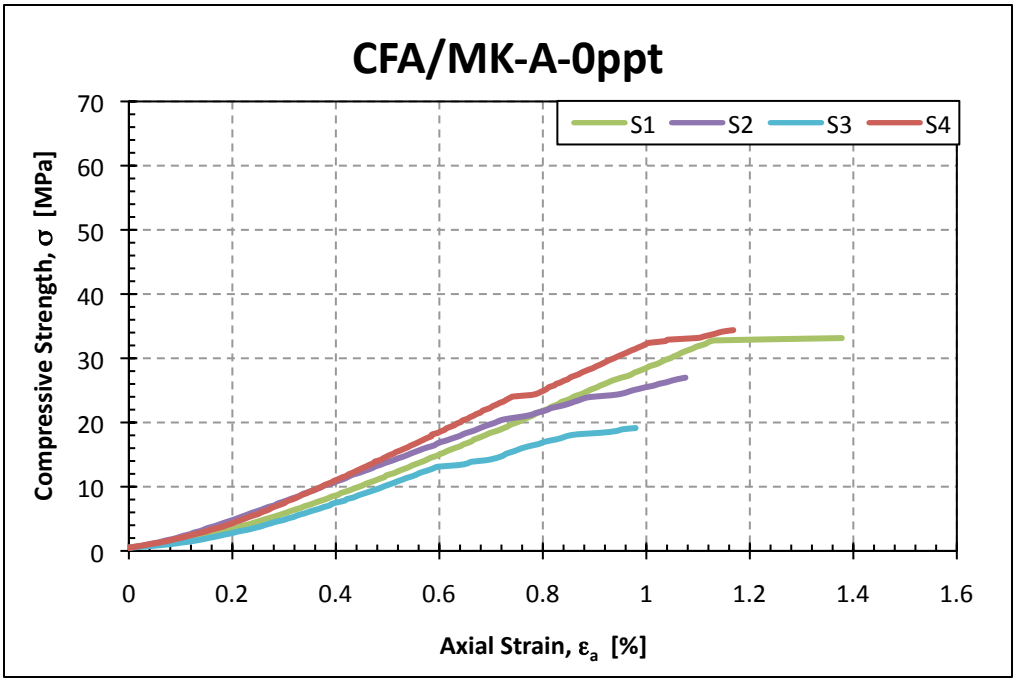

Figure 4.6 Plot of compressive strength versus percent strain for geopolymer cement specimens cured in 0 ppt curing environment.

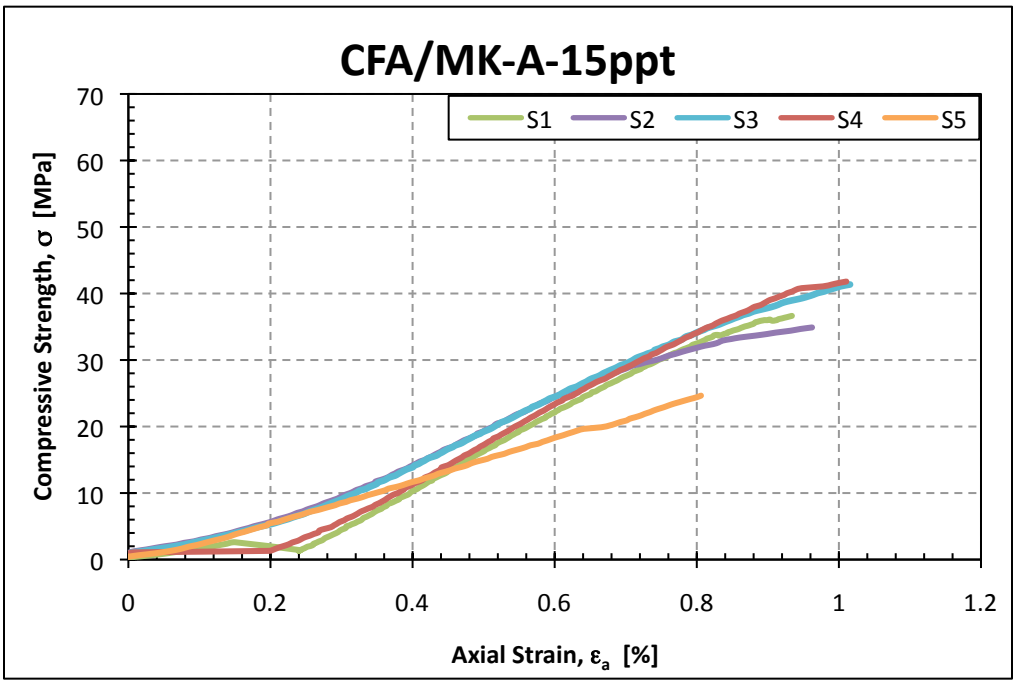

Figure 4.7 Plot of compressive strength versus percent strain for geopolymer cement specimens cured in 15 ppt curing environment.

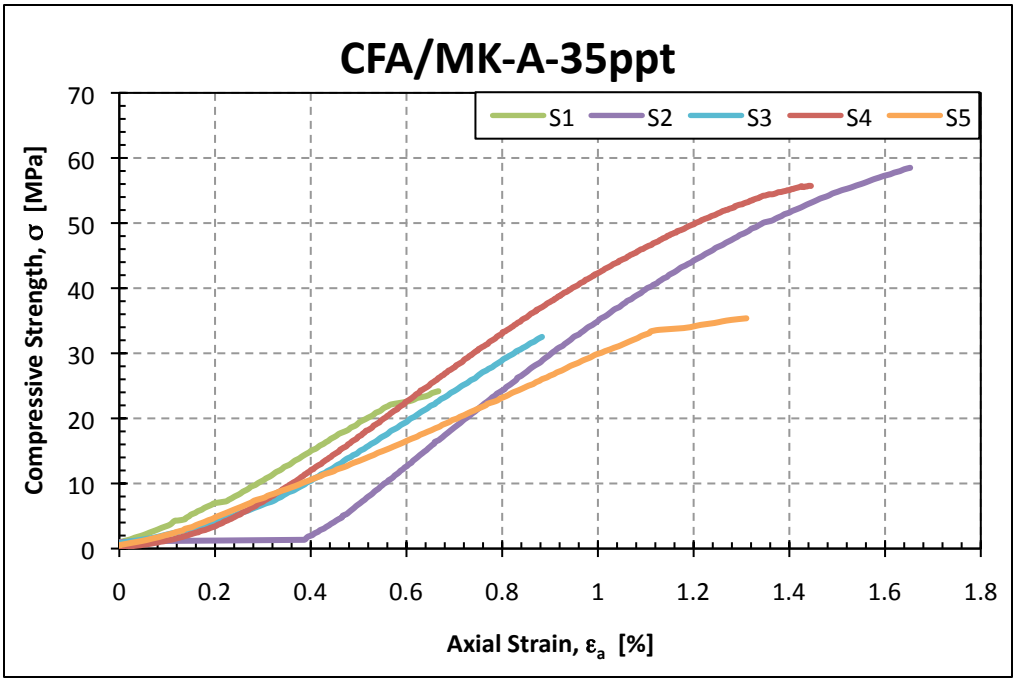

Figure 4.8 Plot of compressive strength versus percent strain for geopolymer cement specimens cured in 35 ppt curing environment.

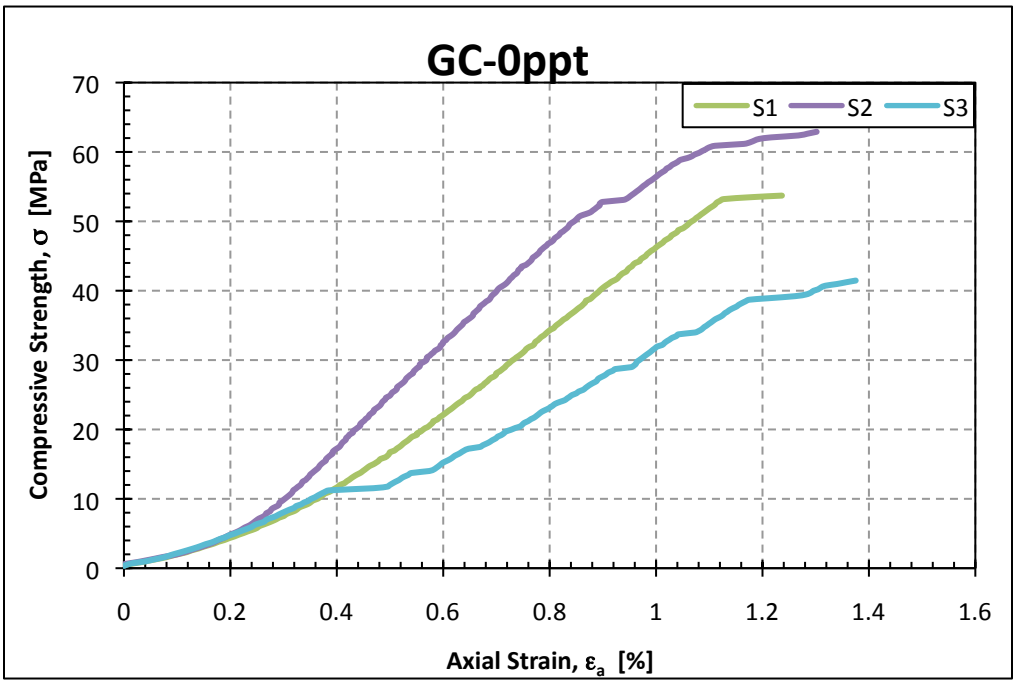

Figure 4.9 Plot of compressive strength versus percent strain for Class G cement specimens cured in 0 ppt curing environment.

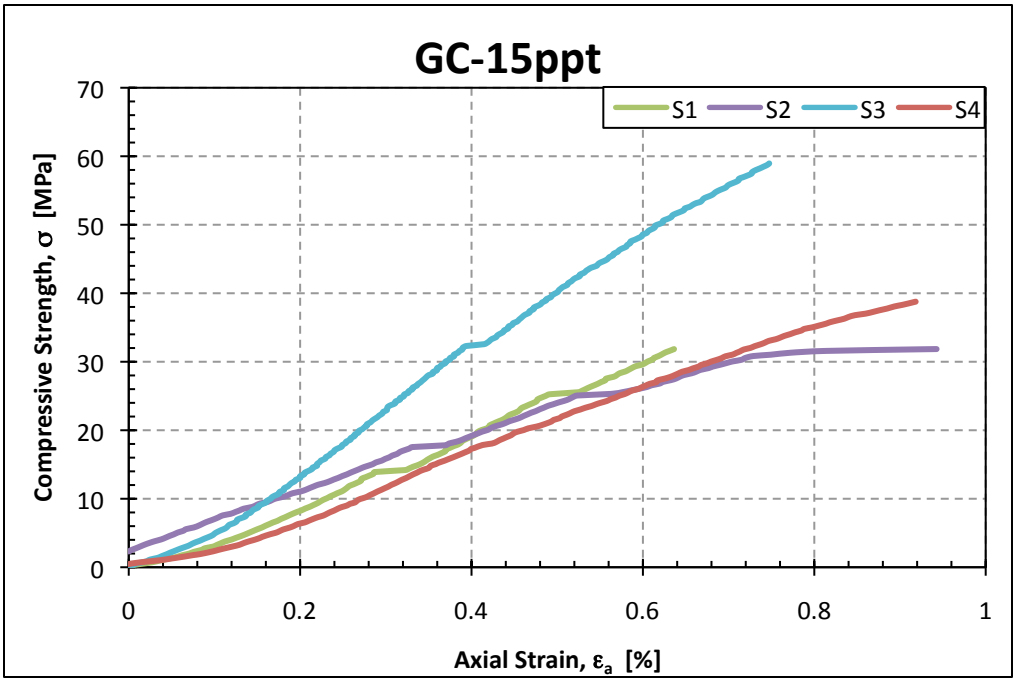

Figure 4.10 Plot of compressive strength versus percent strain for Class G cement specimens cured in 15 ppt curing environment.

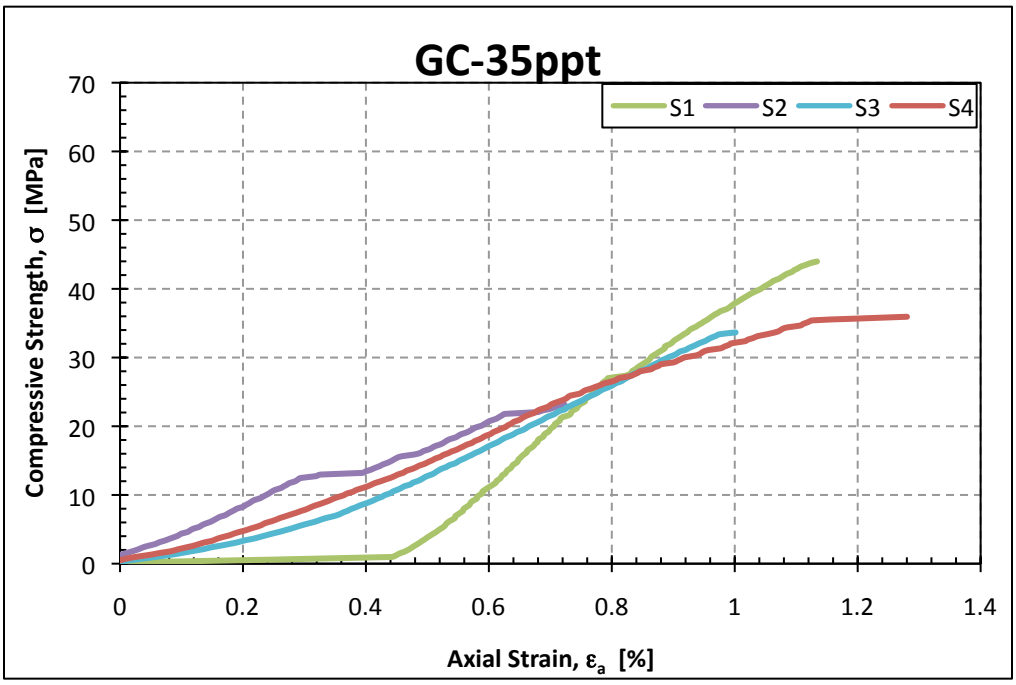

Figure 4.11 Plot of compressive strength versus percent strain for Class G cement specimens cured in 35 ppt curing environment.

Table 4.2 presents a summary of specimens that exhibited the highest compressive strength for each curing environment and cement type. The highest compressive strength achieved for the geopolymer cements occurred at 58.5 MPa for a specimen cured in the 35 ppt environment. Figure 4.12 presents the range of compressive strengths for the cement specimens cured in the different salinities. There is an increasing trend in strength with increased curing salinity for the geopolymer cement specimens. The highest compressive strength achieved for the Class G cements occurred at 62.9 MPa for a specimen cured in the 0 ppt environment. For the Class G cement specimens, Figure 4.12 presents a decreasing trend in strength with increasing salinity. The trends observed for the strengths of the geopolymer and Class G cements for varying saline environments are similar to those observed in the study by Giasuddin et. al (2013).

Figure 4.13 presents the range of failure strains for the cement specimens tested. The failure strains for the geopolymer cement specimens were highest for the 35 ppt curing environment and lowest for the 15 ppt curing environment. The Class G cement presented the highest failure strains for the specimens cured in the 0 ppt curing environment and the lowest for the 15 ppt curing environment.

Figure 4.14 presents the range Young's modulus that was obtained from the stress-strain relationships that were plotted in Figures Figure 4.6 through Figure 4.11. The maximum modulus was obtained for both cement types cured in the 15 ppt saline water. The maximum values of Young's modulus for the geopolymer and Class G cements were 5.54 and 7.60, respectively.

Figure 4.15 presents the range of bulk densities obtained for the cement specimens. For both cement types, the bulk density decreases with decreasing salinity.

Therefore the highest bulk density for the geopolymer and Class G cement were 1.54 g/cm^3 and 1.96 g/cm^3, respectively. The loss in density with decreased salinity could be due to an increased rate of leaching of materials from the cements.

In order to further study the controlling factors that influence the strength and other properties evaluated in the section, compositional and microstructural analysis were performed. The results were later used to determine the validity of the leaching theory.

Table 4.2 Summary table of specimens that exhibited the highest compressive strength for each curing environment and cement type.

Sample		Peak Compressive Strength (MPa)
CFA/MK-A	0ppt-S4	34.4
	15ppt-S4	41.8
	35ppt-S2	58.5
GC	0ppt-S2	62.9
	15ppt-S3	59.0
	35ppt-S1	44.0

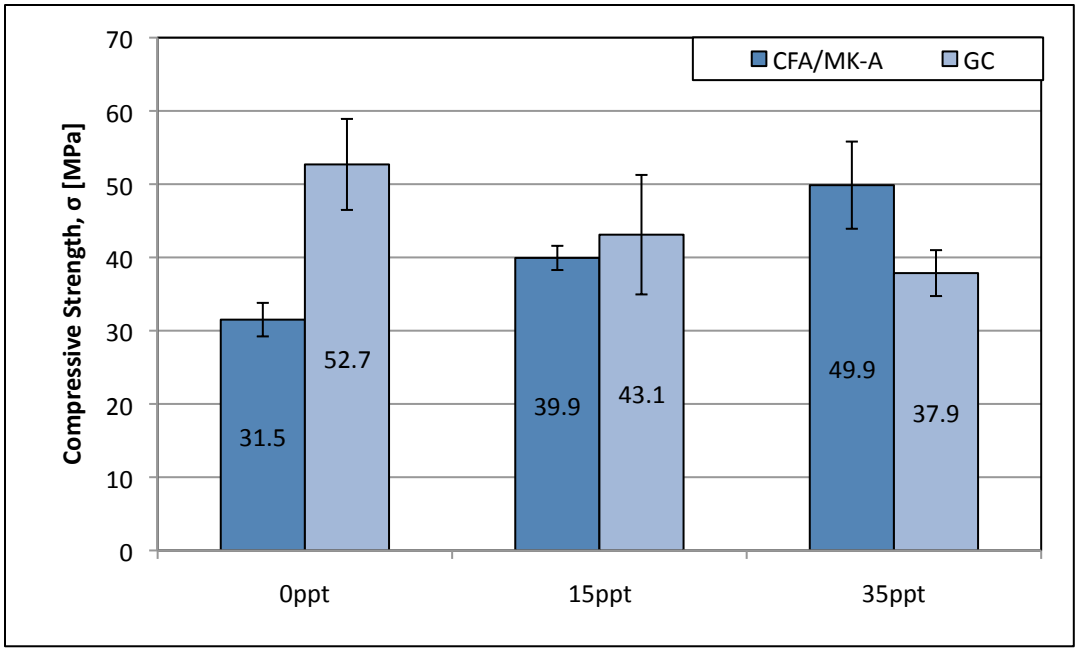

Figure 4.12 Summary of average compressive strengths obtained for the CFA/MK-A geopolymer and Class G cement specimens.

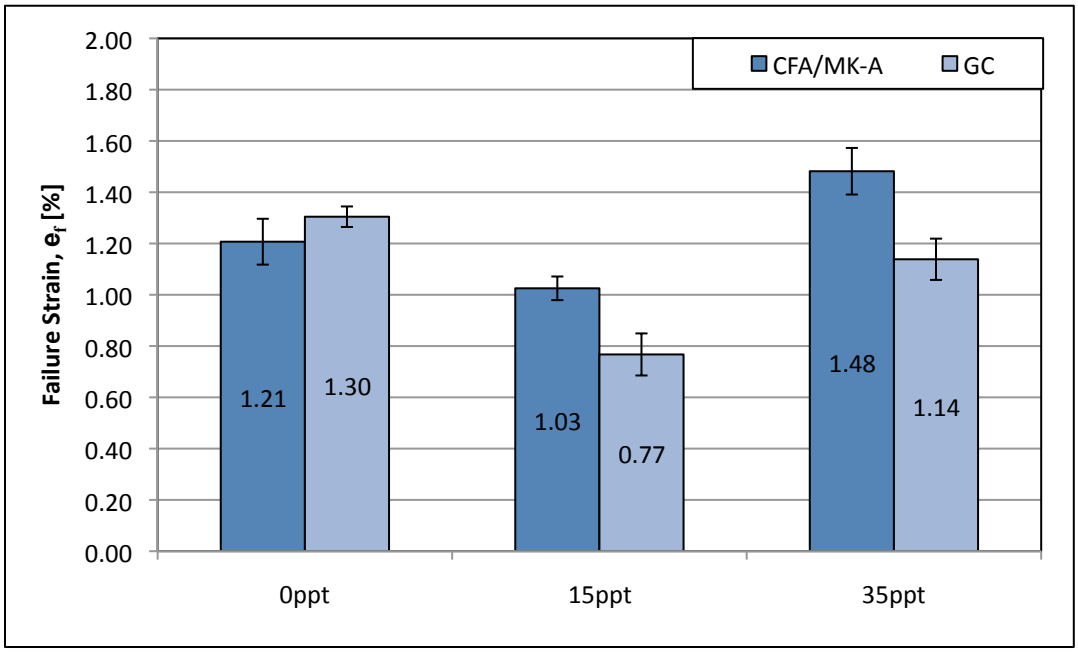

Figure 4.13 Summary of failure strains obtained for the CFA/MK-A geopolymer and Class G cement specimens.

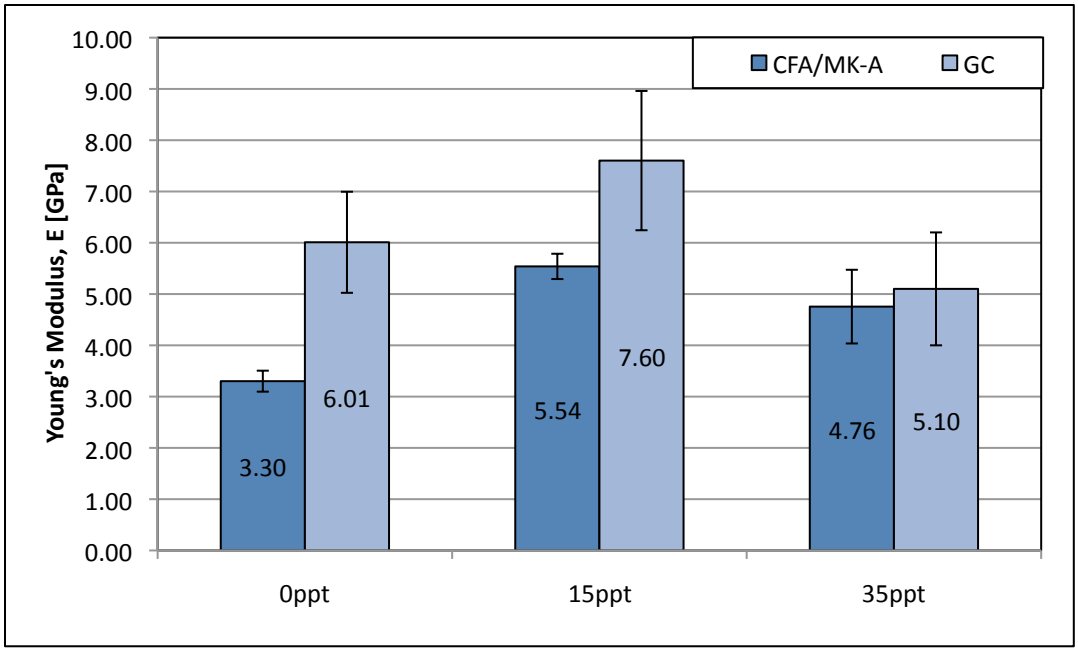

Figure 4.14 Summary of Young's modulus obtained for the CFA/MK-A geopolymer and the Class G cement specimens

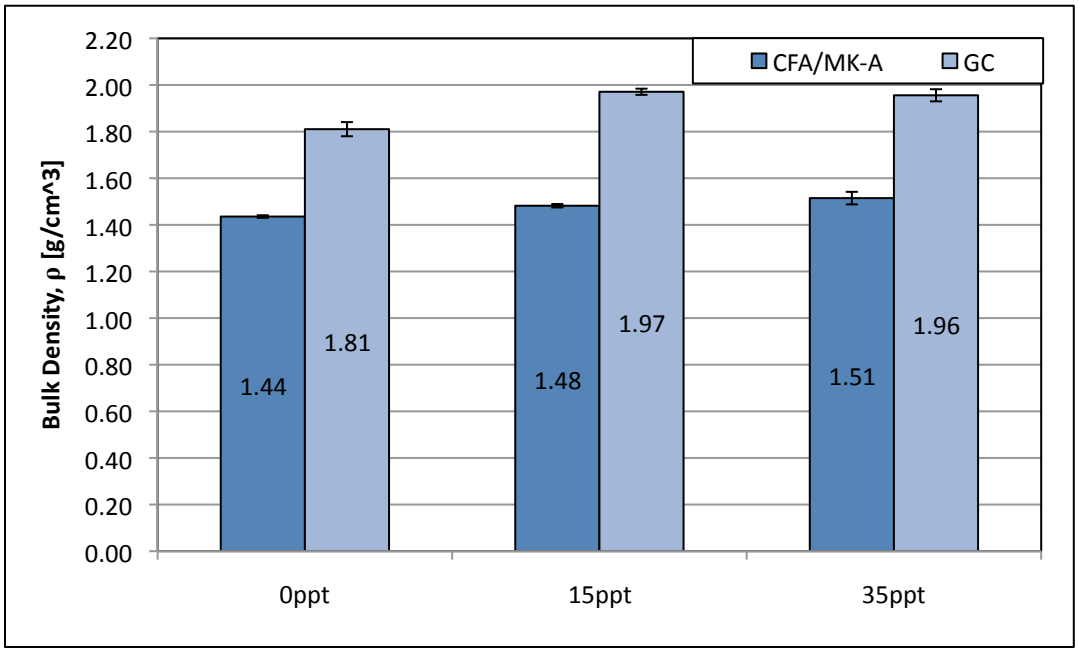

Figure 4.15 Summary of bulk densities obtained for the CFA/MK-A geopolymer and Class G cement specimens

5 ANALYSIS OF COMPOSITION

5.0 Introduction

A compositional analysis was carried out on the cement to provide additional explanation and understanding into the behavior of the different cements during the unconfined compression testing, to determine if any leaching of material had occurred, and to identify the elemental and mineral composition. This analysis was carried out through X-ray fluorescence (XRF), X-ray diffraction (XRD), and pH testing of the curing waters. The following sections will discuss a general introduction into the method of analysis, the details of sample preparation and analysis, the results, and general conclusions.

5.1 Materials and Methods

5.1.1 Materials

Elemental and mineral compositional analyses were performed on the specimens that exhibited the highest unconfined compressive strength for each cement type and curing environment (Table 4.2). The raw materials from which the cements were derived were also analyzed. Differences in composition were further analyzed through pH testing of the curing water prior to commencement of curing and after completion of curing.

5.1.2 XRF

The elemental chemical analysis was performed using a Siemens MRS400 MP and a Philips PW2400 X-ray fluorescence spectrometer. The analysis was performed

through the Geoscience Department at the University of Massachusetts Amherst to identify and quantify the mass percent of major elements as oxides in each specimen. The Siemens spectrometer was utilized for the majority of the analysis. The Phillips spectrometer was utilized for sole purpose of obtaining a more accurate measurement of sodium. Prior to utilizing the XRF spectrometers, each sample was powdered, using a McCrone Micronising Mill, and then fused into glass disks.

5.1.2.1 Sample Preparation

5.1.2.2 Preparation of Powdered Samples

In order to perform the XRF analysis, the cement specimens selected for analysis had to be powdered and fused into glass discs. Each cement specimen was crushed into a powdered sample by utilizing a McCrone Micronising Mill (Figure 5.1). Prior to utilizing the mill, the maximum particle size of each sample had to be 0.5 mm. Particles above 0.5 mm were reduced in a percussion mortar and sieved through the sieve included in the McCrone Sample Preparation Kit. The material that was able to pass through the sieve was then reduced in the mill using the wet grinding technique.

The wet grinding technique required the crushed and sieved sample to be placed in a jar containing grinding elements that were ordered in an array of 6 rows of 8. Next, approximately 7 mL of propan-2-ol (Isopropyl alcohol) was poured over each sample and the lid of the jar was securely screwed on to prevent leakage. The jar was then inserted into the mill and the sample was ground in the mill for a minimum of 4 minutes. Once grinding was completed, the jar was removed from the mill and the lid was replaced with a two hole pouring lid. The sample was then wet sieved, using RO water, through a sieve

with a 45 μm opening into a beaker. To ensure the sample had been completely transferred from the jar to the beaker, 15 mL of grinding liquid was added and the jar was vibrated for an additional 15 seconds. Once again the lid of the jar was removed and replaced with the two hole pouring lid and the remaining contents were poured through the sieve. This process was repeated until the jar was adequately cleaned. Finally, the sieved contents within the beaker were dried in an oven at approximately 110 ˚C.

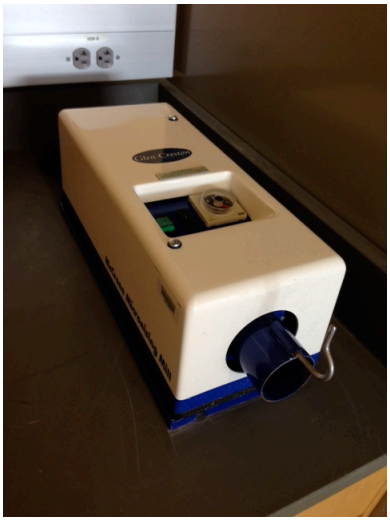

Figure 5.1 McCrone Micronising Mill.

5.1.2.3 Preparation of Fused Glass Disks

In order to analyze the selected samples using XRF, each sample had to be prepared and fused into two glass disks. By creating two disks for each sample, a check into the agreement between the results could be utilized as an indication for whether the samples were properly prepared and to further verify the results.

After the powdered samples were prepared, approximately 2 grams of sample was measured, placed into a crucible, and ignited in a furnace at 850 ˚C over night. After

ignition, the sample was cooled. Once cool, approximately 0.3000±0003 g of the sample was weighed out into a sample jar. Next, approximately 1.6070±0005 g of a Fluxite GX-47 X-ray Flux was added to the jar. This flux was composed of the following: 47.0% Lithium Tetraborate ($Li_2B_4O_7$), 36.7% Lithium Carbonate (Li_2CO_3), 16.3% Lanthanum Oxide (La_2O_3). One pill of ammonium oxide ($(NH_4)O_2$) was added to the admixture of sample and flux to serve as a releasing again. The sample jar was then rotated at a 45˚ angle until the contents were well mixed. The contents were transferred to a metal crucible and then placed into a furnace at a temperature of approximately 1050 ˚C. After two minutes the crucible was removed from the furnace with tongs, swirled to further mix the contents, and returned to the furnace. This process of removal and mixing was repeated until the crucible had remained in the furnace a total of 6 minutes. After this period, the crucible was removed from the furnace and the molten contents were poured into a graphite mold that had been heating on a hot plate to 232 ˚C. Once in the mold, a press was placed over the sample, the contents solidified, and a glass disc was produced. The disc was transferred to another hot place and to anneal overnight. Once fully cooled, the discs were ready for analysis.

5.1.3 XRD

The XRD analysis was performed through the Department of Civil Engineering at MIT to provide qualitative information on the mineral content for the selected specimens. Chunwei Ge, a PhD student at MIT, agreed to assist with running the analysis on the samples. XRD patterns were obtained in a PANalytical X'Pert PRO Multipurpose X-ray Powder Spectrometer, using CuKα (λ= 1.542515 Å) radiation generated at 1.8 kW (45

kV, 40 mA) (Figure 5.2). All scans used a 0.25° divergence slit, a step size of 0.017° 2θ, a scan speed of 0.017° per 90 s, and a continuous scan range of 5-64° 2θ.

Figure 5.2 PANalytical X'Pert PRO Multipurpose X-ray Powder Spectrometer.

5.1.3.1 Sample Preparation

A minimum of 5 grams of dried powdered sample was required for XRD analysis. The powdered samples were prepared following the procedure described in Section 5.1.2.2. Once powdered and thoroughly dried, the samples were placed in 5 mL plastic vials and sent to MIT for analysis.

5.1.4 pH

In order to monitor leaching of chemical components, the pH of the curing water was obtained prior to the start of curing and after the completion of curing. The pH taken

before the start of curing was obtained as a reference value for the water where zero leaching had occurred.

5.1.4.1 Materials

The pH was obtained for each curing water prior to contact with the cement specimens. As previously mentioned, these values were considered a reference for a situation where zero leaching had occurred. After the 28-day curing duration, the cement specimens were removed from the curing waters and the pH was taken for each environment.

5.1.4.2 pH Testing

The pH was acquired using a Mettler Toledo SevenCompact S220 pH meter (Figure 5.3a). The buffer solutions used to calibrate the meter possessed a pH of 4.00, 7.00, and 10.00 (Figure 5.3b).

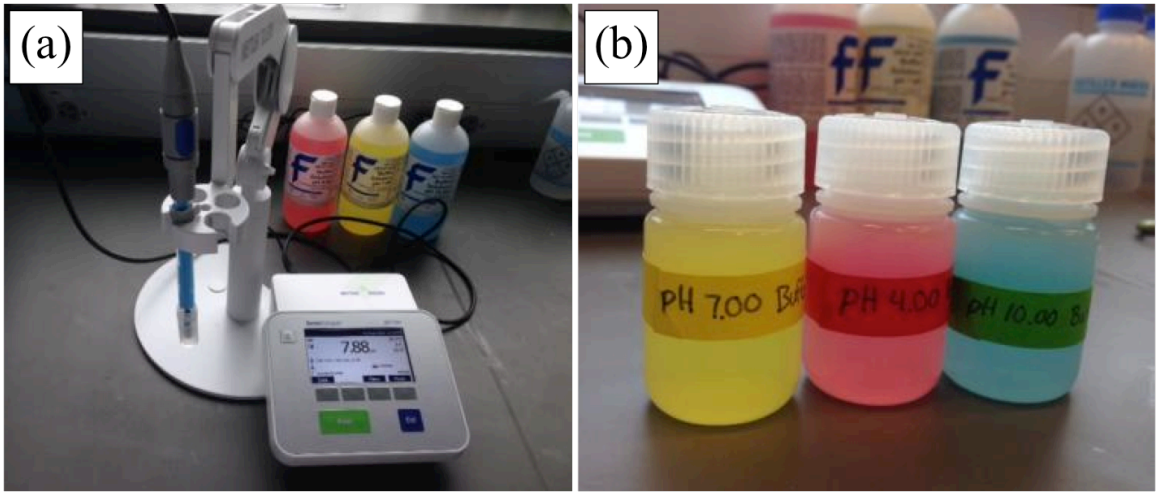

Figure 5.3 (a) pH meter used for testing (b) pH buffer solutions.

5.2 Results and Discussion

5.2.1 XRF

Table 5.1 summarizes the averaged results, given in percent mass, for chemical analysis of each sample. The molar ratios of Si/Al and Na/Si were calculated from the average results and are presented in Table 5.2. Overall, the ratio of Si/Al showed a decreasing trend with decreasing salinity for the geopolymer cement and ranged from 1.79 to 1.83. The Na/Si ratio of the geopolymer cement increased with decreasing salinity and ranged from 0.229 to 0.244. For the Class G cement, the Si/Al ratio was 4.92 for the 15 ppt and 35 ppt cured samples and increased to 4.94 for the 0 ppt cured sample. There was no significant variation in Na/Si ratio for the Class G cement for the three curing conditions and the Class G cement dry mix (GC dry mix) and was approximately zero for all. A significant increase was observed in the Si/Al ratio for the GC dry mix. While the Class G cement exhibited ratios of Si/Al ranging from 4.92 to 4.94, the GC dry mix possessed a ratio of 4.69. This indicated that leaching was present during water curing.

The increasing Si/Al and decreasing Na/Si with decreasing salinity indicated that the rate of leaching increased with decreasing salinity for the geopolymer cement. While the Class G cement did not present significant differences in the ratio of Si/Al and Na/Si for the different curing environments, there was a slight increase observed for the 0 ppt cured specimens. This slight increase and a notable increase in Si/Al between the Class G dry mix and the cement supported the theory that leaching had occurred during water curing for both cements.

It should be noted that the ratios of Si/Al and Na/Si for the 35 ppt geopolymer cements were observed to be closest to those calculated for the CFA/MK-A design mix. The ratio of Si/Al was 1.78 for the design mix and 1.79 for the 35 ppt cured geopolymer cement. The ratio of Na/Si was 0.25 for the design mix and approximately 0.24 for the geopolymer cement. This indicates that the cured geopolymer cement was closest to the true design and displayed the lowest amount of leaching when cured in the 35 ppt environment.

Table 5.1 Summary of sample chemical composition given in percent mass.

Oxides	CFA/MK-A			GC			Raw Materials		
	0ppt-S4	15ppt-S4	35ppt-S2	0ppt-S2	15ppt-S3	35ppt-S1	CFA	MK	GC Dry Mix
SiO_2	50.65	51.77	51.12	22.14	21.85	21.78	37.93	53.80	17.75
TiO_2	1.21	1.20	1.16	0.24	0.23	0.22	1.45	1.39	0.20
Al_2O_3	23.44	24.28	24.18	3.80	3.77	3.76	19.99	40.11	3.21
Fe_2O_3	3.77	3.73	3.58	4.93	4.82	4.78	6.78	2.00	4.18
MnO	0.02	0.02	0.02	0.12	0.13	0.12	0.04	0.003	0.10
MgO	2.17	1.97	1.91	1.07	0.85	0.93	5.01	0.08	0.93
CaO	10.00	9.59	9.35	58.68	58.04	58.20	22.55	0.04	63.61
Na_2O	5.99	6.22	6.44	0.02	0.00	0.00	1.60	0.02	0.004
K_2O	0.35	0.36	0.35	0.17	0.12	0.10	0.52	0.29	0.19
P_2O_5	0.57	0.57	0.57	0.03	0.05	0.04	1.23	0.16	0.02
Total	98.18	99.72	98.70	91.21	89.85	89.93	97.09	97.89	90.20

Table 5.2 Molar ratio of Si/Al and Na/Si for each sample analyzed using XRF.

Sample	Molar Ratio Si/Al	Molar Ratio Na/Si
CFA/MK-A-0ppt-S4	1.83	0.229
CFA/MK-A-15ppt-S4	1.81	0.233
CFA/MK-A-35ppt-S2	1.79	0.244
GC-0ppt-S2	4.94	0.001
GC-15ppt-S3	4.92	0.000
GC-35ppt-S1	4.92	0.000
CFA Raw Material	1.61	0.082
MK Raw Material	1.14	0.001
GC Dry Mix	4.69	0.000

5.2.2 XRD

Figure 5.4 presents XRD patterns for the Class G dry mix, metakaolin, and Class C fly ash that was used as source materials for the cements. The XRD pattern of the metakaolin exhibits a pronounced broad hump between 18-32° 2θ with a few sharp peaks. This indicates that the metakaolin principally contains amorphous silica and alumina. The crystalline phases were magnetite, magnesium, quartz, and portlandite. The Class G dry mix presents a minor hump between 30-35° 2θ with main mineral components of the Class G dry mix were gypsum, dolomite, calcium carbonate, quartz, and lime. The XRD pattern of the Class C fly ash exhibited a less pronounced broad hump between 20-36° 2θ with a few sharp peaks. This indicates that the fly ash is predominately composes of amorphous phases. The crystalline phases were mullite, quartz, anhydrite, and magnetite.

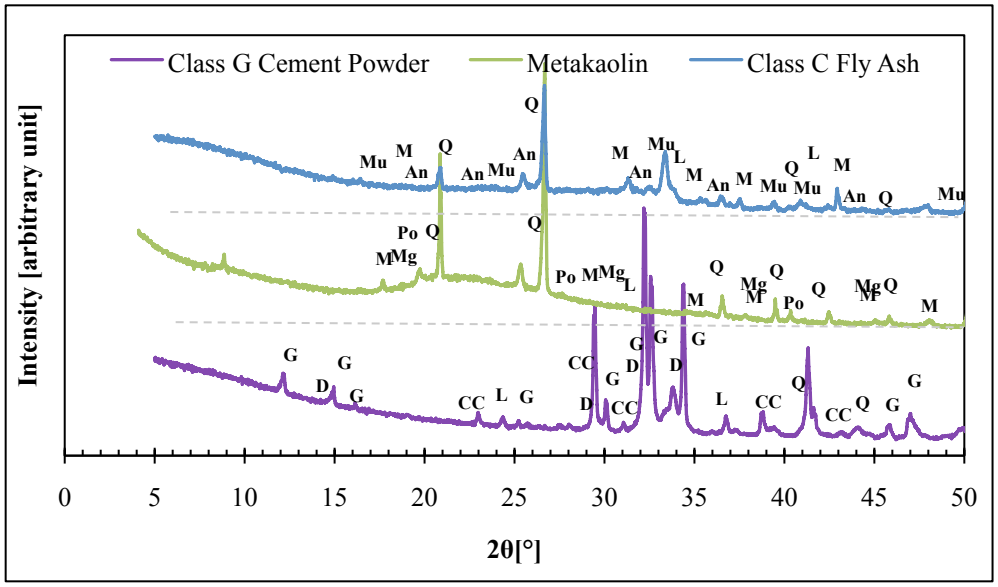

Figure 5.4 XRD patters for Class G cement powder, metakaolin, and Class C fly ash (An = anhydrite, CC = calcium carbonate, D = dolomite, G = gypsum, L = lime, M = magnetite, Mg = magnesium dialuminum oxide, Mu = mullite, Po = Portlandite, Q = quartz).

Figure 5.5 presents XRD pattern for the geopolymer cements cured in the different saline conditions. The XRD patterns show a broad hump between 20-37° 2θ with a few sharp peaks for each geopolymer. This indicates that amorphous phases are dominant at large quantities and crystalline phases are also present. These crystalline phases include andradite, anhydrite, brucite, calcite, periclase, and quartz. The minerals presents in all three geopolymers were brucite, calcite, and quartz. The similarity in the broad reflection between the geopolymers cured in different saline conditions indicates that the same degree of geopolymerization occurred for each. In addition to these finding, the XRD patterns did not indicate any invasion of salt crystals in the geopolymer cements.

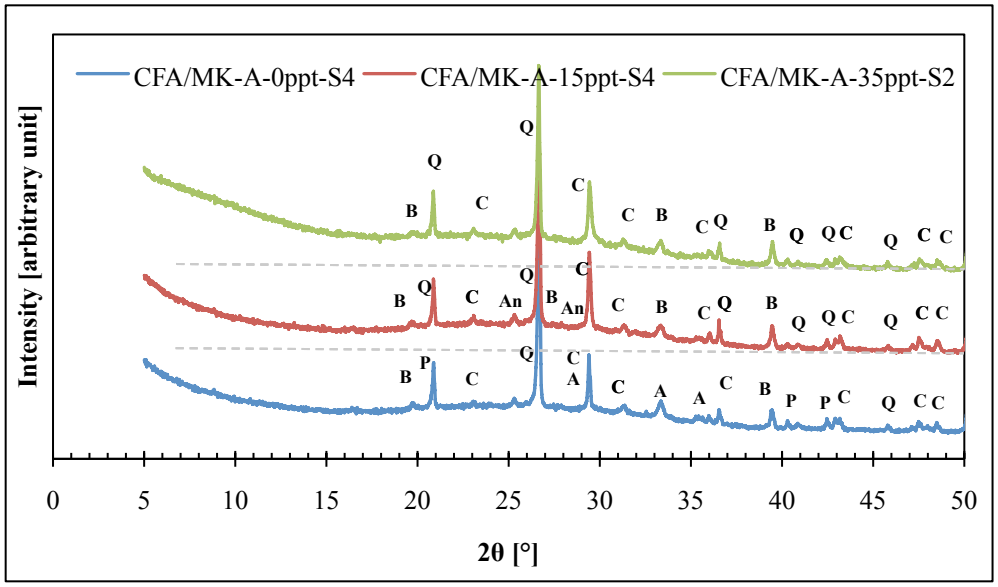

Figure 5.5 XRD patterns of geopolymer cement specimens (A = andradite, An = anhydrite, B = brucite, C = calcite, P = periclase, Q = quartz).

Figure 5.6 presents the XRD patterns for the Class G cements cured in the different saline conditions. The XRD patterns show a multiple sharp peaks in all of the cements. The Class G cement cured in the 0 ppt environment possessed crystalline phases of dolomite, katoite, portlandite, calcite, and brucite. The cement cured in the 15 ppt environment possessed crystalline phases of calcium hydroxide, brucite, quartz, and calcite. The cement cured in the 35 ppt environment possessed crystalline phases of calcite, calcium carbonate, and portlandite. The presence of more crystalline phases with decreased salinity could be due to leaching of material out of the cement during curing and a reduction in the overall reaction of the material. This would result in a higher presence of crystalline phases.

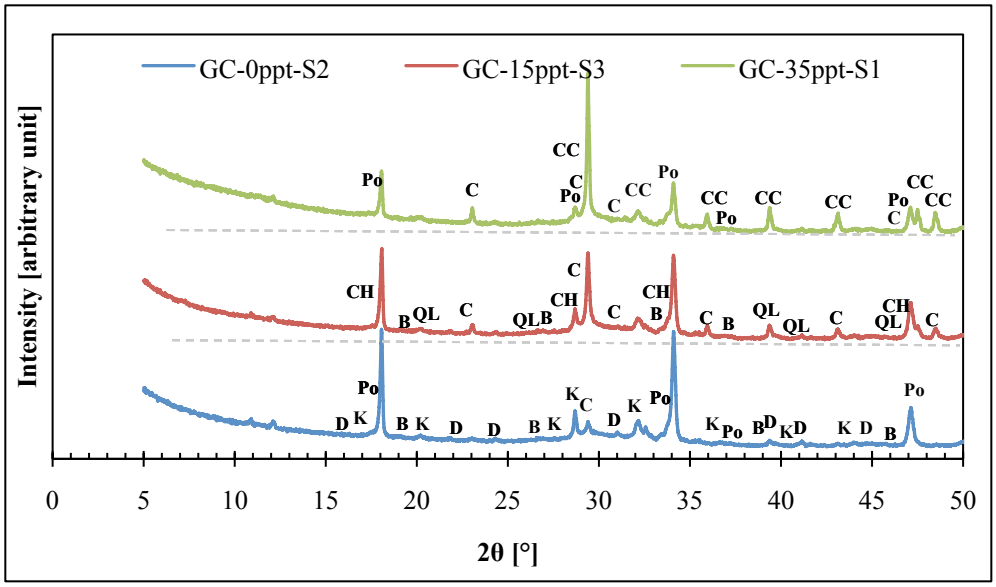

Figure 5.6 XRD patterns for Class G cement specimens (B = brucite, C = calcite, CC = calcium carbonate, CH = calcium hydroxide, D = dolomite, K = katoite, L = lime, Po = portlandite, QL = quartz low).

5.2.3 pH

Figure 5.7 presents the average and range of pH values obtained for the different curing environments for the cements. Figure 5.8 presents the values shown in Figure 5.7 and presents them next to the reference pH that was obtained for the different curing waters. It was observed that the pH of both the geopolymer and Class G cements increased with decreasing salinity. The values of pH for the curing water deviates the greatest from the reference for the 0 ppt curing environment and the least for the 35 ppt curing environment. The increase in pH for decreased salinity indicated that leaching was present during curing and that the rate of leaching increased with decreasing salinity. The increasing deviation from the reference with decreasing salinity supported this theory.

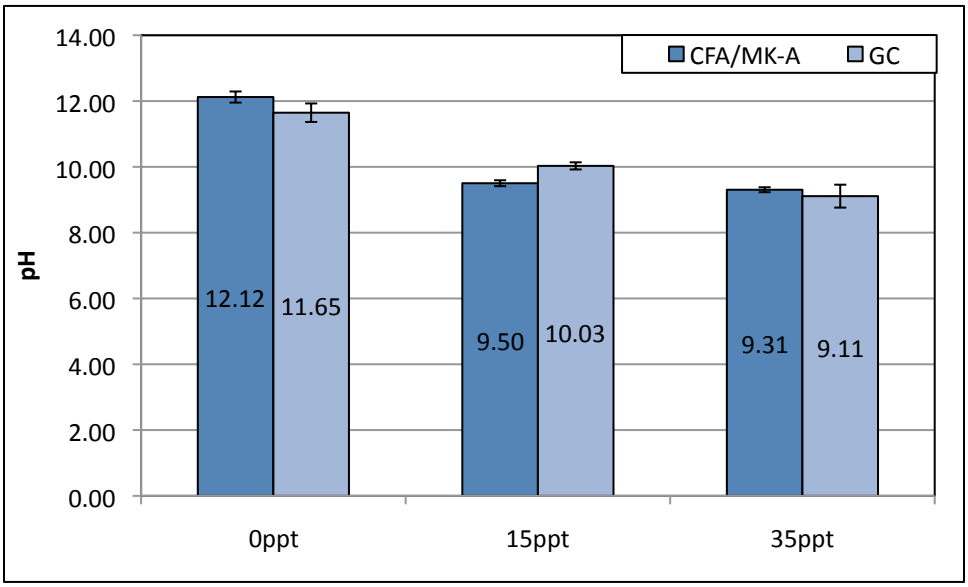

Figure 5.7 Summary of pH values obtained for curing waters after 28 days of specimen water curing.

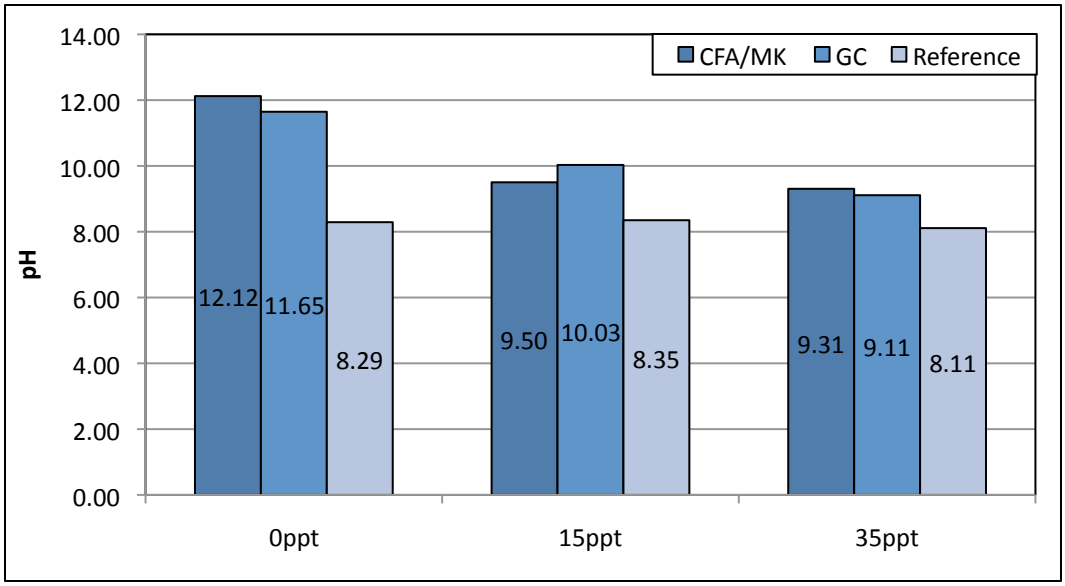

Figure 5.8 Summary of pH values for curing waters before the start of curing and after the 28 days of specimen water curing.

6 CHARACTERIZATION OF MICROSTRUCTURE

6.0 Introduction

A microstructural analysis was carried out on the geopolymer cement samples to provide information into the micromorphology of the material, in addition to a qualitative analysis of the elemental composition. The following sections discuss the material, methods, and results of this analysis.

6.1 Materials and Methods

6.1.1 Materials

The microstructural analysis was performed on the cured geopolymer cement specimens that exhibited the highest unconfined compressive strengths for the different curing environments. The samples were obtained from the cement cores that were exposed after unconfined compression testing.

6.1.2 SEM/EDS

The micromorphology of the geopolymer cement specimens was observed using a FEI Magellan 400 XHR-SEM high resolution scanning electron microscope featured with an Oxford X-MAX 80 mm^2 Energy Dispersive X-ray Spectrometer for element mapping. The following sections include information on sample preparation and methodology for performing the analysis.

6.1.2.1 Sample Preparation

For the microstructural analysis, small pieces of cement were selected from the cylindrical specimens that were failed under unconfined compression testing and examined. These cement pieces were obtained from the core of the cylinders with the objective of only analyzing the cement that was representative of the entire geopolymer specimen. The external cement surfaces were avoided due to potential differences in microstructure from contact with curing water. Once selected, the cement pieces were dried in an oven at approximately 110 ˚C for a minimum of 24 hours. The drying was performed to eliminate excess moisture that might interfere with the clarity of the images obtained.

6.1.2.2 SEM/EDS Testing

Prior to performing the analysis, the dried samples were mounted to a 25.4 mm pin mount using carbon tape (Figure 6.1). When performing an SEM analysis, it is common practice to coat nonconductive specimens with very thin coating of electrically conductive material. This is done to prevent charging of the specimens, which causes scanning faults and low quality images. However, coating samples with conductive materials can produce an inaccurate qualitative analysis of the elemental composition. In addition to this, coating the samples would result in reduced definition of pores. For these reasons, it was decided that the geopolymer cement specimens would remain uncoated for the analysis. In order to compensate for the lack of conductive coating, copper tape was wrapped along the edges to the samples (Figure 6.1).

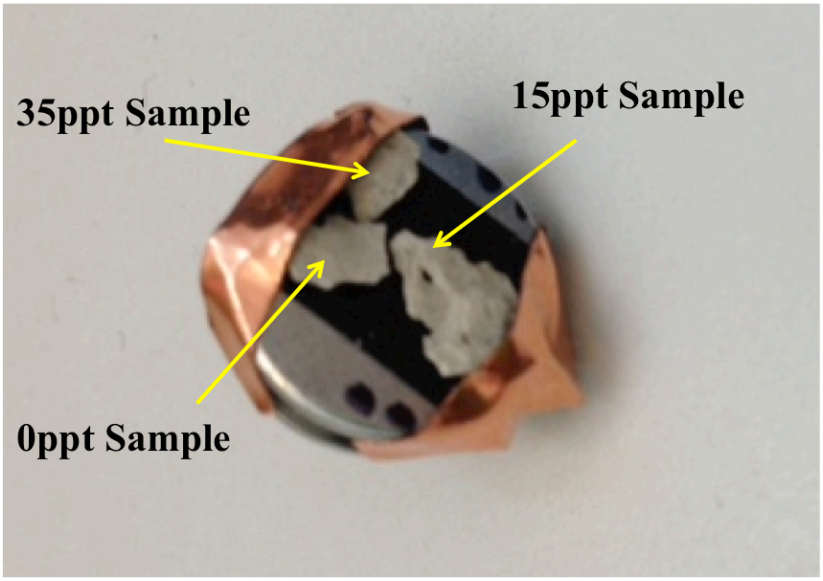

Figure 6.1 Geopolymer cement samples mounted for SEM/EDS analysis.

As mentioned earlier, a Magellan 400 was utilized for the analysis (Figure 6.2a). Once the samples were mounted and the copper tape was in place, the pin mount was placed within the chamber of the microscope, advanced to the desired positon, and the analysis was carried out (Figure 6.2b).

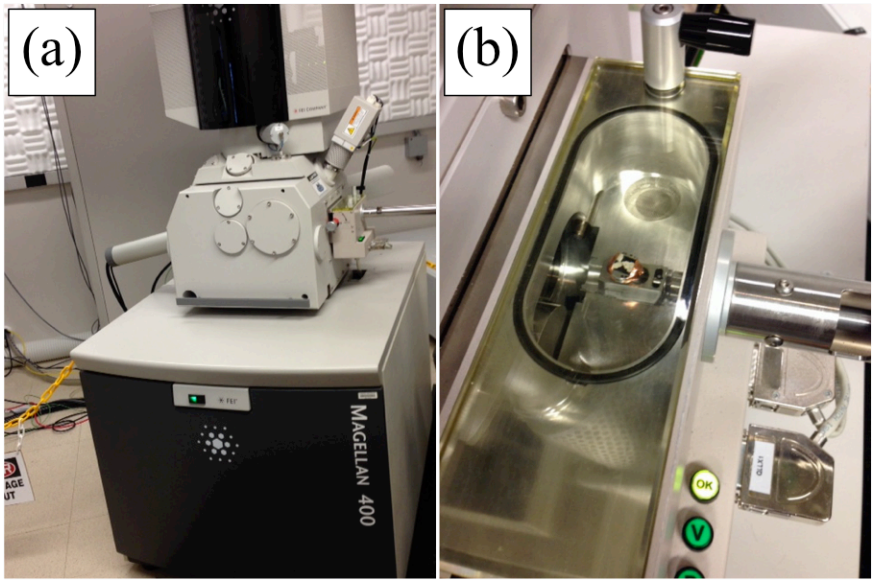

Figure 6.2 (a) Magellan 400; (b) Sample mount within chamber.

6.1.3 Porosity

The porosity of each cement sample was analyzed using the SEM micrographs obtained. A general range of pore sizes were identified, using AutoCAD 2015, by referencing the scale and measuring selected pores from SEM micrographs with magnifications ranging from 500 nm to 1000 nm. It should be noted that this method of determining pore size was not statistical and was performed simply to gain further insight into the differences between the selected geopolymer cement samples.

6.2 Results and Discussion

6.2.1 SEM

6.2.1.1 General Microstructure

The images acquired through SEM were utilized to gain information on the porosity of the geopolymer matrix material. Figures Figure 6.3, Figure 6.4Figure 6.5 present the SEM micrographs for the different samples. All samples, regardless of curing condition, presented unreacted and partially reacted components within the fully reacted matrix. Partially reacted fly ash is presented in Figures Figure 6.3b, Figure 6.4b and c, andFigure 6.5c. Unreacted fly ask and metakaolin are shown in Figure 6.3c and Figure 6.5b, respectively. Overall there was not a large difference in the general microstructures of geopolymer cements cured in different salinities.

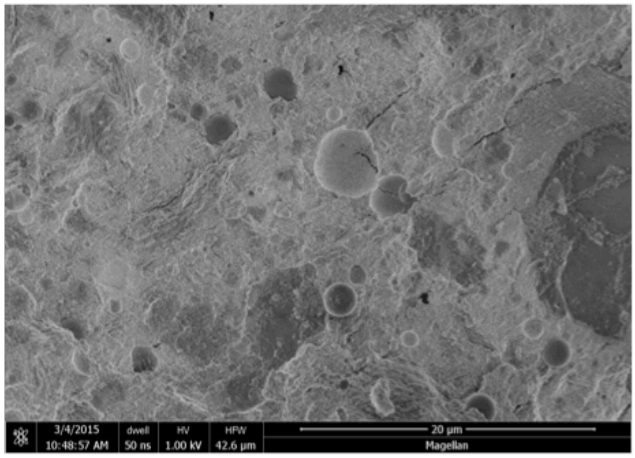

(a)

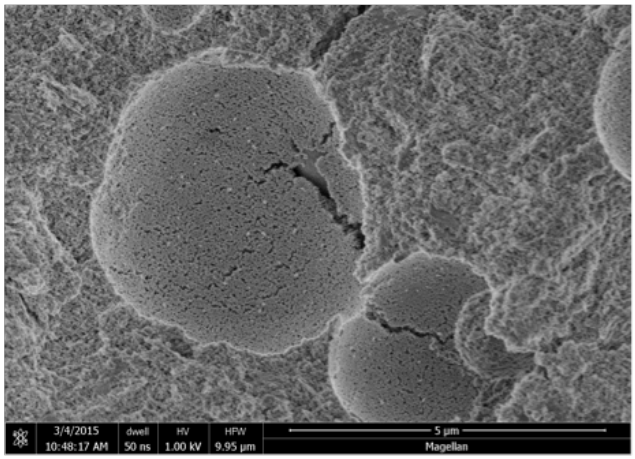

(b)

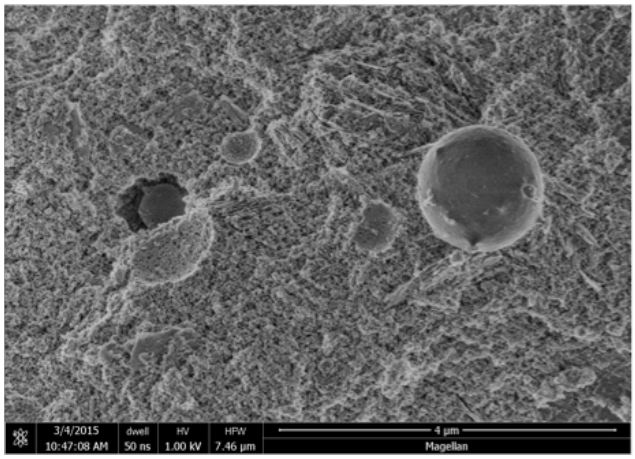

(c)

Figure 6.3 SEM micrographs of geopolymer cement sample from 0 ppt water cured specimen: (a) Overall structure; (b) area showing partially reacted fly ash and (c) area showing unreacted fly ash.

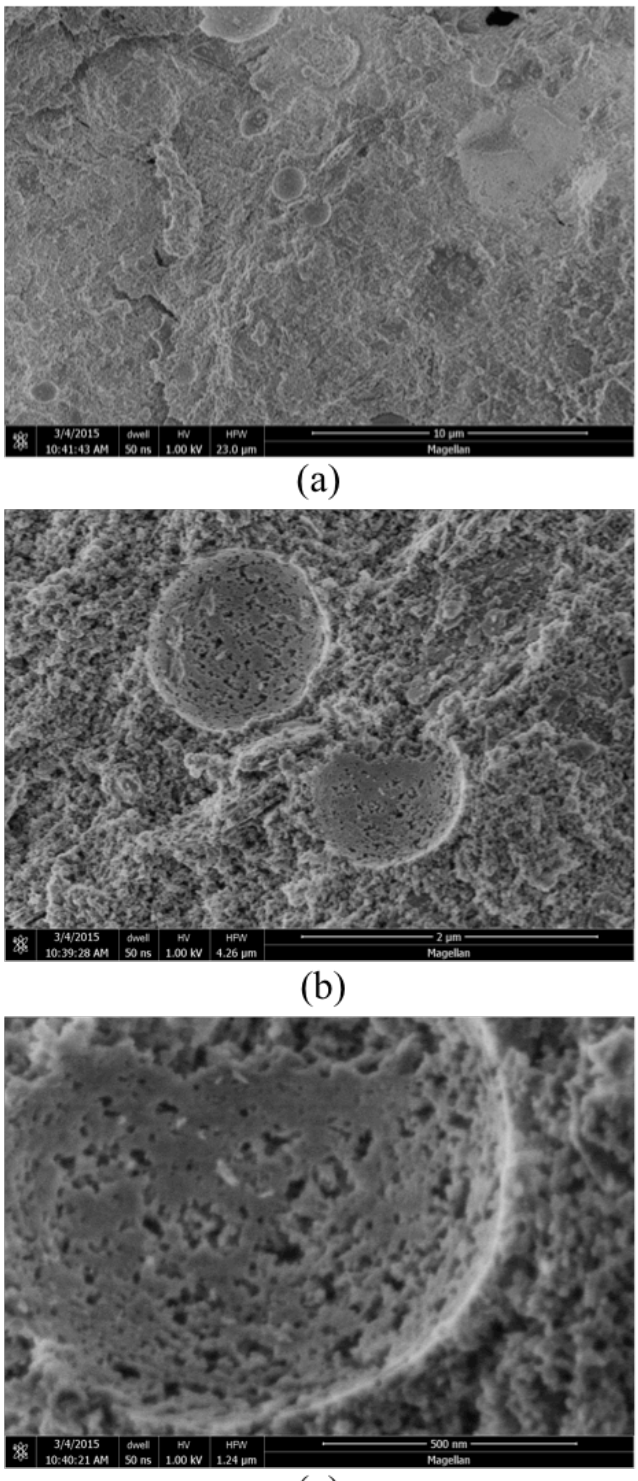

Figure 6.4 SEM micrographs of geopolymer cement sample from 15 ppt water cured specimen: (a) Overall structure; (b) area showing two partially reacted fly ash spheres and (c) magnified view of unreacted fly ash.

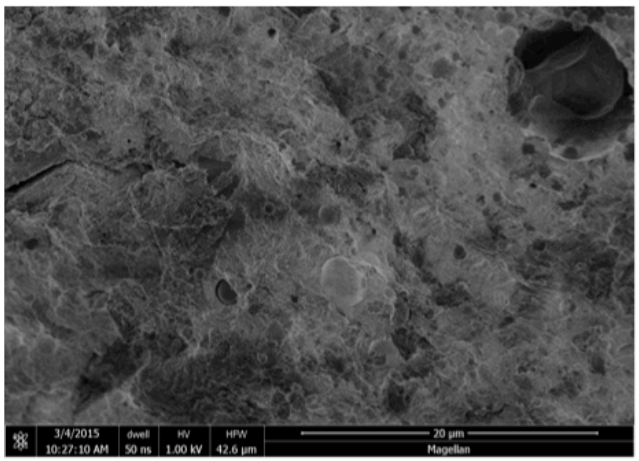

(a)

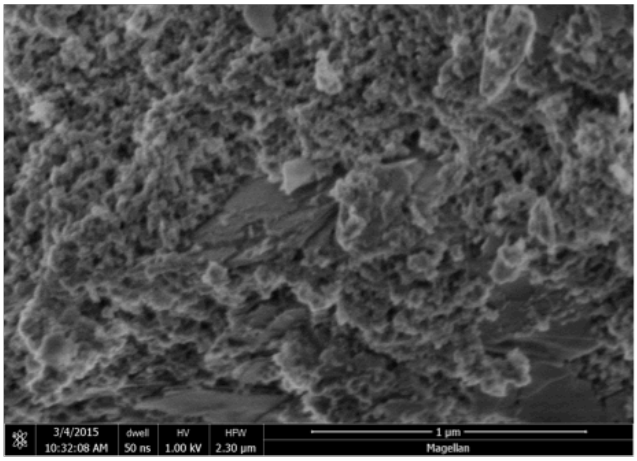

(b)

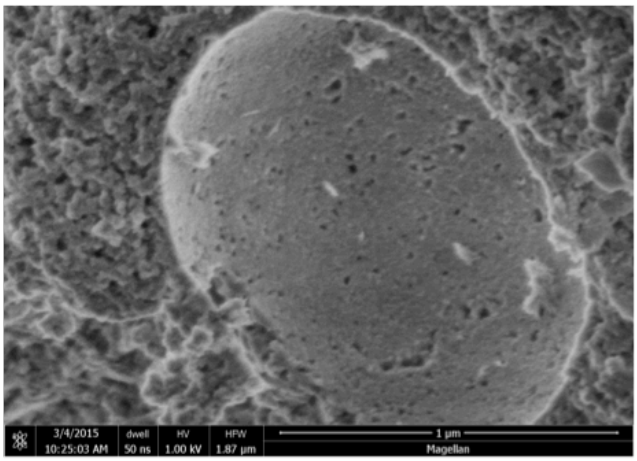

(c)

Figure 6.5 SEM micrographs of geopolymer cement sample from 35 ppt water cured specimen: (a) Overall structure; (b) magnified area showing unreacted metakaolin and (c) Magnified area showing partially reacted fly ash.

6.2.1.2 Noteworthy Features

Figure 6.6 presents an overview of an SEM micrograph that was taken for a location on the geopolymer cement specimen that was cured in the 35 ppt environment. Figure 6.7 presents magnified views of the locations marked in Figure 6.6. Figure 6.7a presents a magnified view of an octahedral crystal embedded in partially reacted fly ash. Figure 6.7b presents a magnified view of an abnormality observed in the geopolymer matrix.

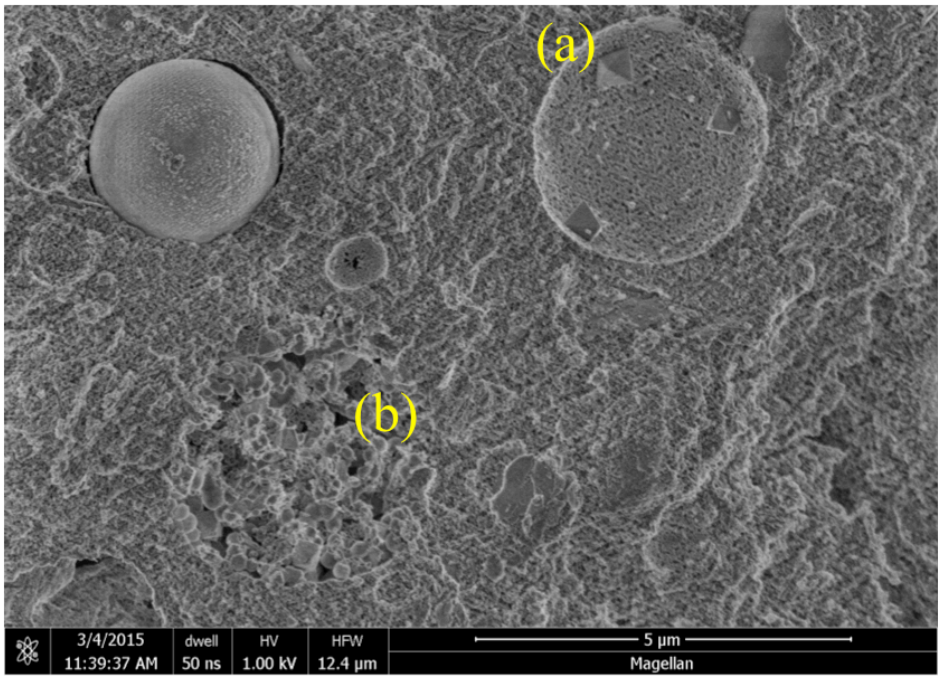

Figure 6.6 SEM micrograph of area in sample where notable features are observed at locations (a) and (b).

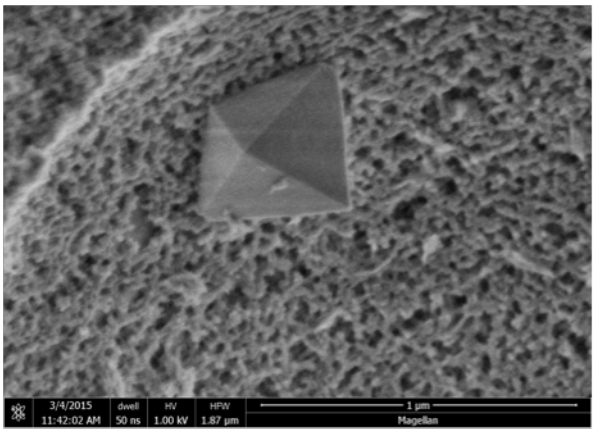

(a)

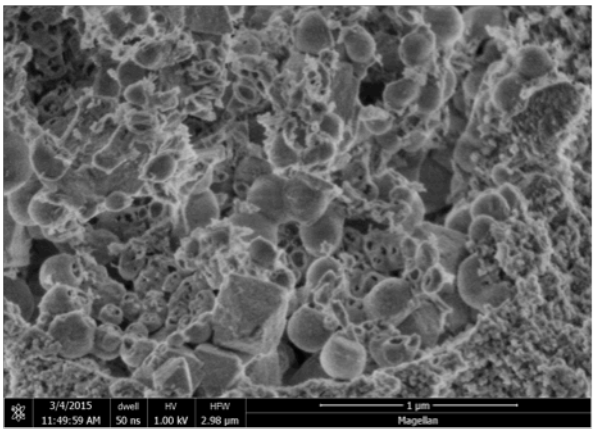

(b)

Figure 6.7 Magnified views of locations marked in Figure 6.6: (a) magnified view of octahedral crystal; (b) magnified view of abnormality in geopolymer matrix.

EDS mapping was performed to further identify the elemental composition of the abnormality in the matrix. The results of this mapping can be observed in Figure 6.8. It was found that the abnormality possessed a high concentration of magnesium (Figure 6.8f). One explanation to what this abnormality might be is a potential impurity within the metakaolin used to derive the geopolymer cement.

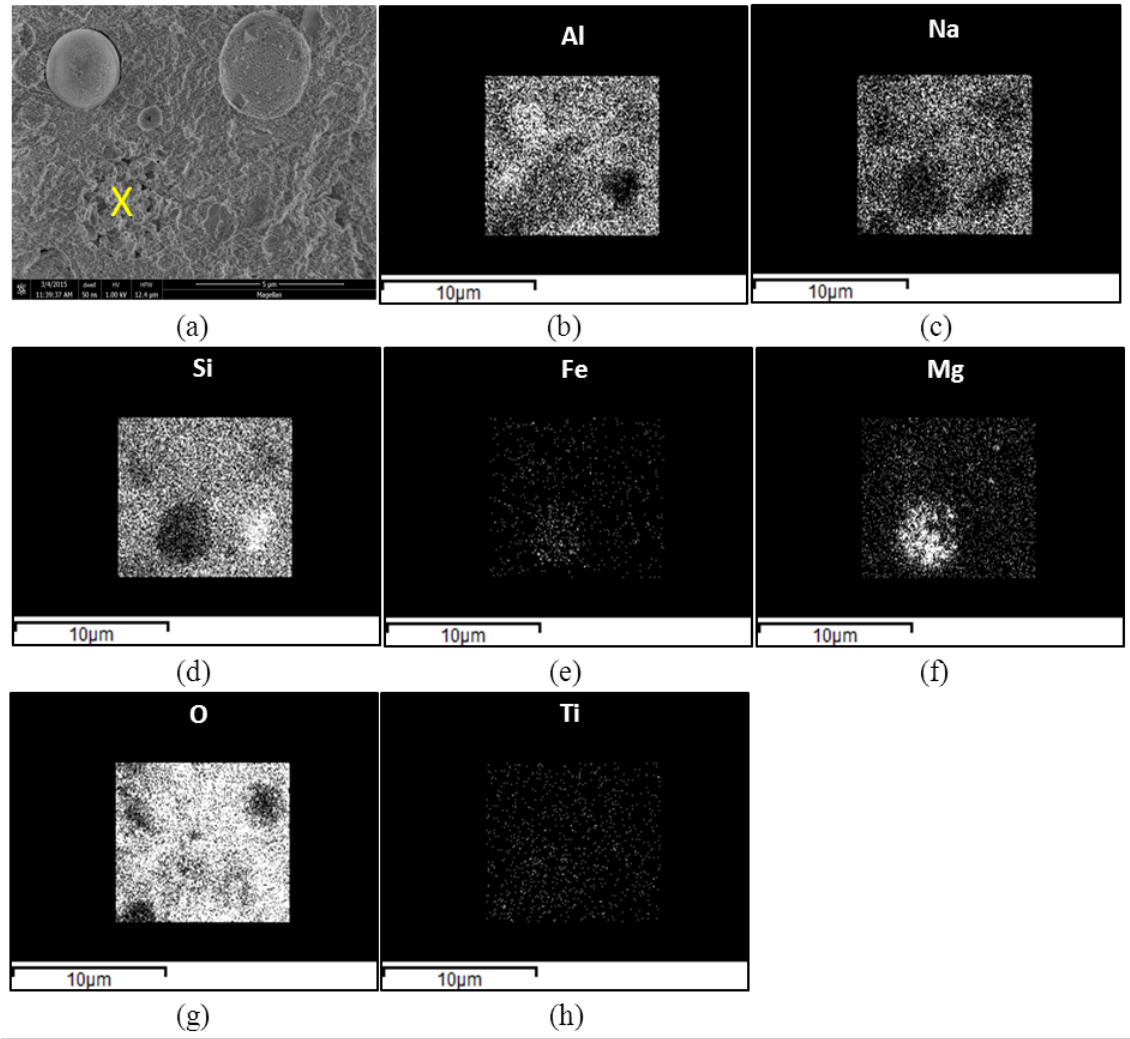

Figure 6.8 EDS mapping of matrix abnormality for 35 ppt geopolymer. (a) SEM micrograph depicting the location of the abnormality for mapping; (b) aluminum map; (c) sodium map; (d) silicon map; (e) iron map; (f) magnesium map; (g) oxygen map; (g) titanium map.

6.2.1.3 Porosity

Figures Figure 6.9Figure 6.10Figure 6.11 present selected measurements of pore size for each geopolymer cement sample. For the 0ppt cured geopolymer cement, the selected range was between 9.67 nm and 27.47 nm. For the 15 ppt cured geopolymer

cement, the selected range was between 13.39 nm and 29.25 nm. For the 35 ppt cured geopolymer cement, the selected range was between 10.27 nm and 26.18 nm. Overall there was no significant different in microstructure of the geopolymer cement for the different curing environments with regards to pore size.

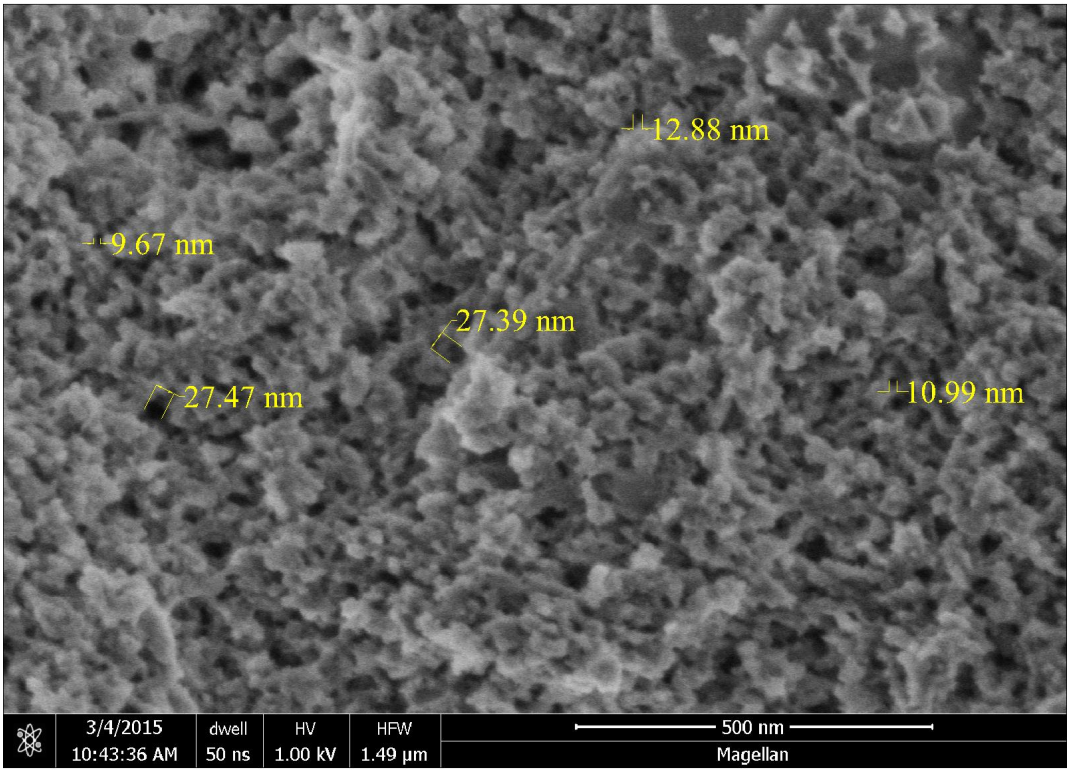

Figure 6.9 SEM micrograph of 0ppt geopolymer cement sample with range of selected pore sizes marked.

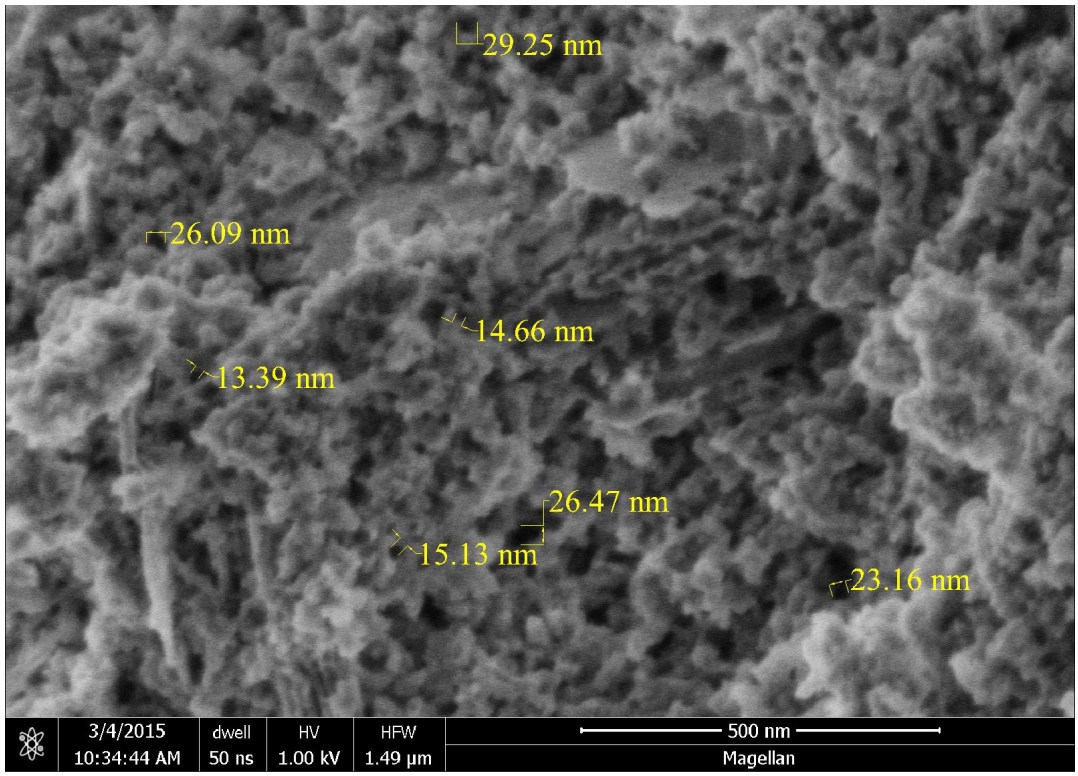

Figure 6.10 SEM micrograph of 15ppt geopolymer cement sample with range of selected pore sizes marked.

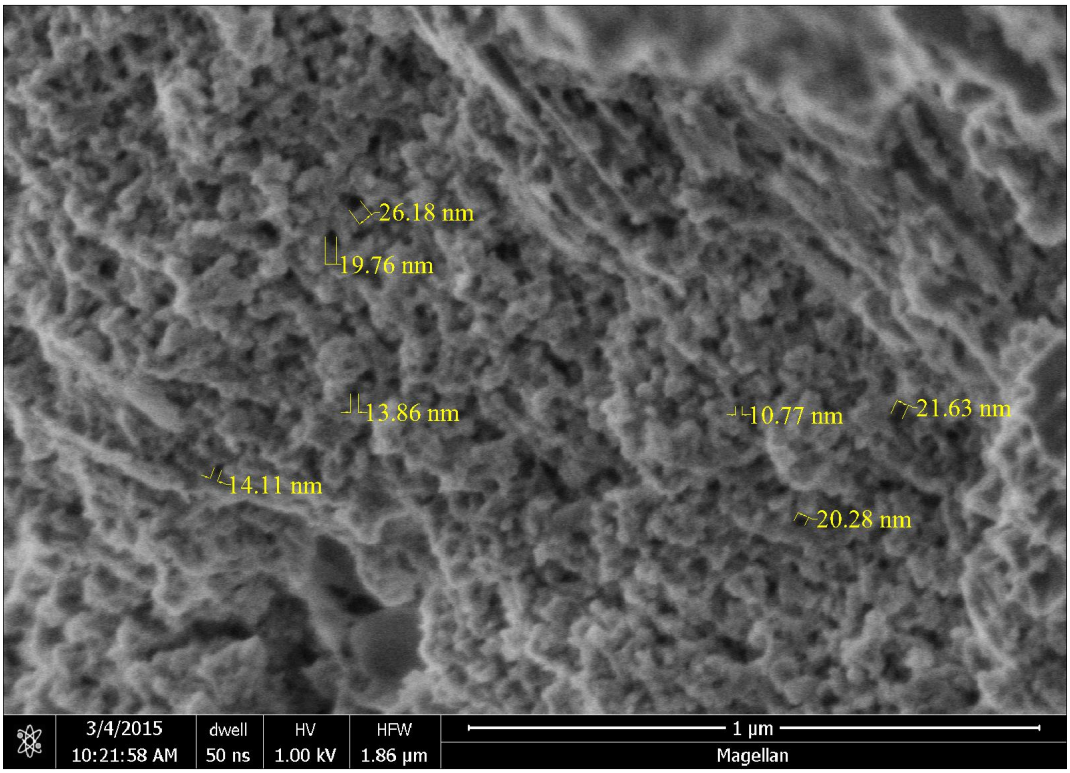

Figure 6.11 SEM micrograph of 35ppt geopolymer cement sample with range of selected pore sizes marked.

6.2.2 EDS

Tables Table 6.1Table 6.2Table 6.3 displays information for the 0 ppt, 15 ppt, and 35 ppt geopolymer cements. Each table presents the locations from which each spectrum was taken and the molar ratios of Si/Al and Na/Si that were subsequently calculated. The locations of each spectrum are noted for the 0 ppt, 15 ppt, and 35 ppt geopolymer cement samples in Figures Figure 6.12, Figure 6.13, and Figure 6.14, respectively. A compilation of the spectrums obtained for each sample are presented in Figures Figure 6.15,Figure 6.16Figure 6.17. For the most part, there appears to be a decrease in Si/Al

and an increase in Na/Si with increasing salinity for the geopolymer matrix. This agrees with the trend observed in the XRF results for the geopolymer cements.

Table 6.1 Summary of spectrum location, molar ratio of Si/Al, and molar ratio of Na/Si for 0 ppt geopolymer cement Specimen 4 sample.

Spectrum	Location	Molar Ratio Si/Al	Molar Ratio Na/Si
1	Partially Reacted Fly Ash	2.06	0.12
2	Geopolymer Matrix	1.89	0.21
3	Boundary	1.94	0.16
4	Unreacted Fly Ash	0.87	0.20
5	Unreacted Fly Ash	0.93	0.37
6	Unreacted Fly Ash	1.49	0.36

Table 6.2 Summary of spectrum location, molar ratio of Si/Al, and molar ratio of Na/Si for 15 ppt geopolymer cement Specimen 4 sample.

Spectrum	Location	Molar Ratio Si/Al	Molar Ratio Na/Si
1	Unreacted Metakaolin	1.41	0.21
2	Unreacted Metakaolin	1.81	0.34
3	Partially Reacted Fly Ash	2.47	0.10
4	Geopolymer Matrix	1.99	0.27
5	Geopolymer Matrix	1.81	0.30
6	Unreacted Metakaolin	1.09	0.20

Table 6.3 Summary of spectrum location, molar ratio of Si/Al, and molar ratio of Na/Si for 35 ppt geopolymer cement Specimen 2 sample.

Spectrum	Location	Molar Ratio Si/Al	Molar Ratio Na/Si
1	Partially Reacted Fly Ash	1.56	0.26
2	Unreacted Fly Ash	0.87	0.32
3	Boundary	1.56	0.33
4	Geopolymer Matrix	0.51	0.46
5	Geopolymer Matrix	0.81	0.16

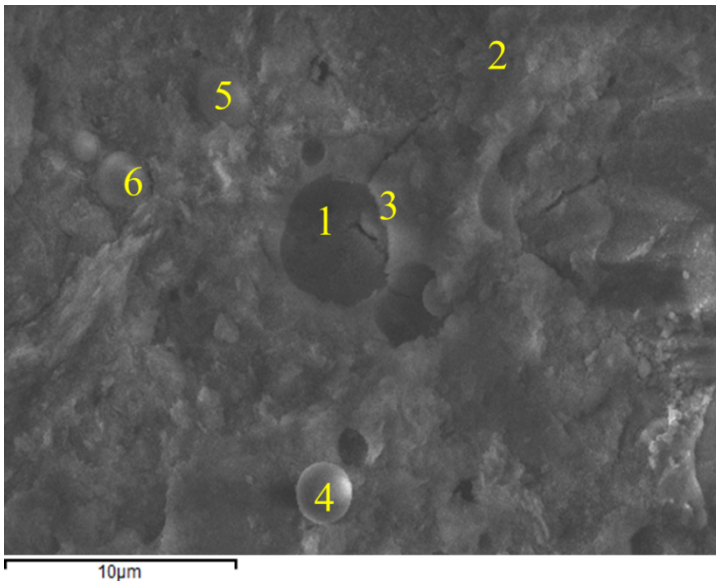

Figure 6.12 EDS spectrum locations for 0 ppt geopolymer cement Specimen 4 sample.

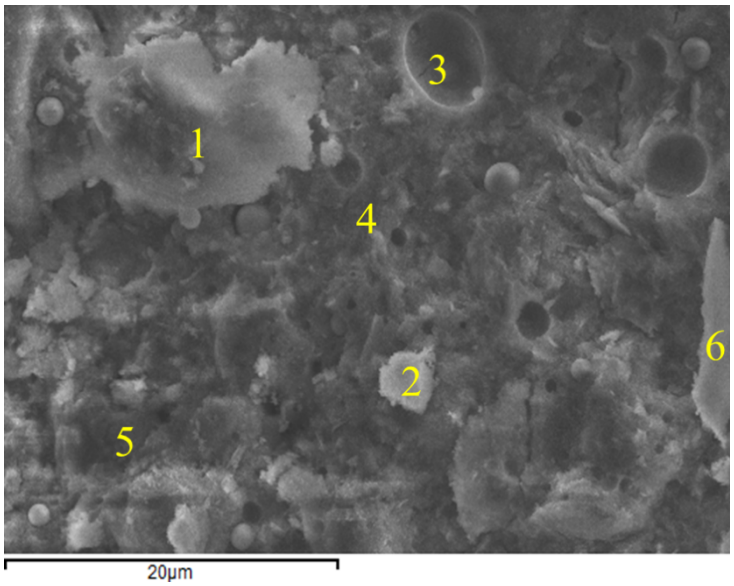

Figure 6.13 EDS spectrum locations for 15 ppt geopolymer cement Specimen 4 sample.

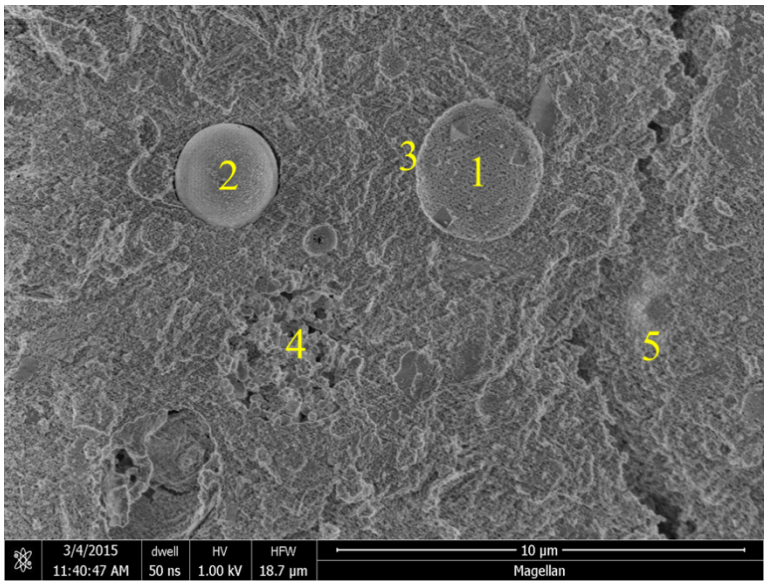

Figure 6.14 EDS spectrum locations for 35 ppt geopolymer cement Specimen 2 sample.

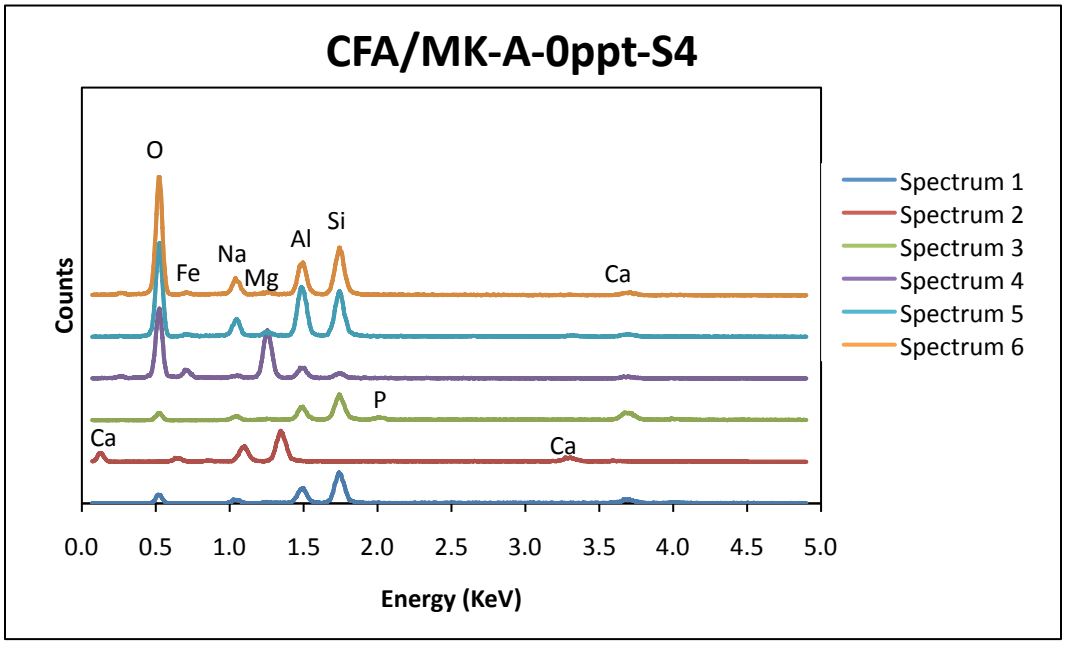

Figure 6.15 EDS spectra for sample obtained from 0 ppt geopolymer cement Specimen 4 sample.

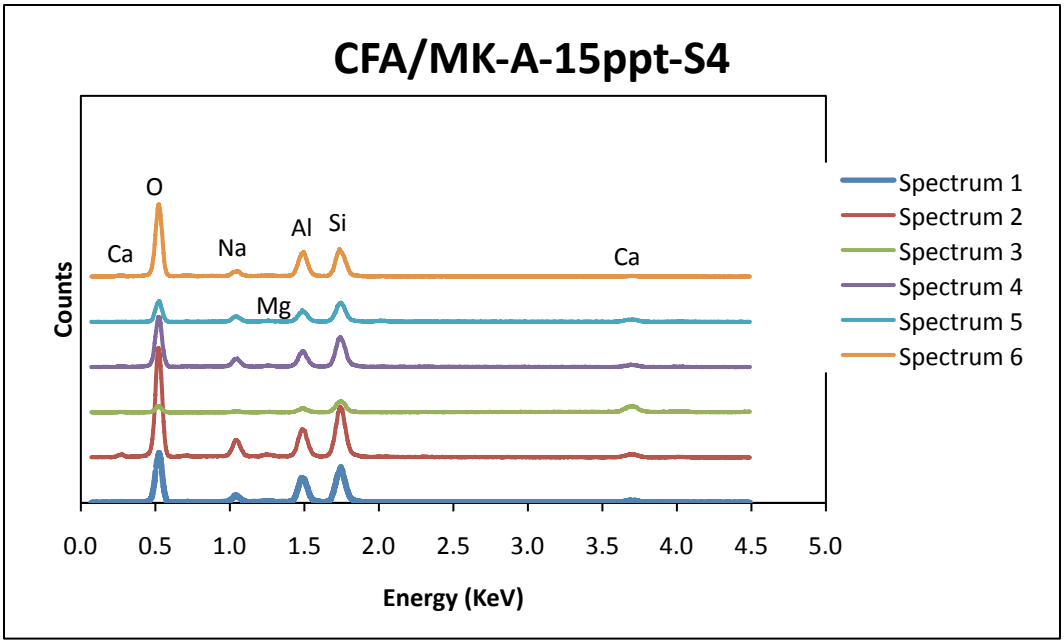

Figure 6.16 EDS spectra for sample obtained from 15 ppt geopolymer cement Specimen 4 sample.

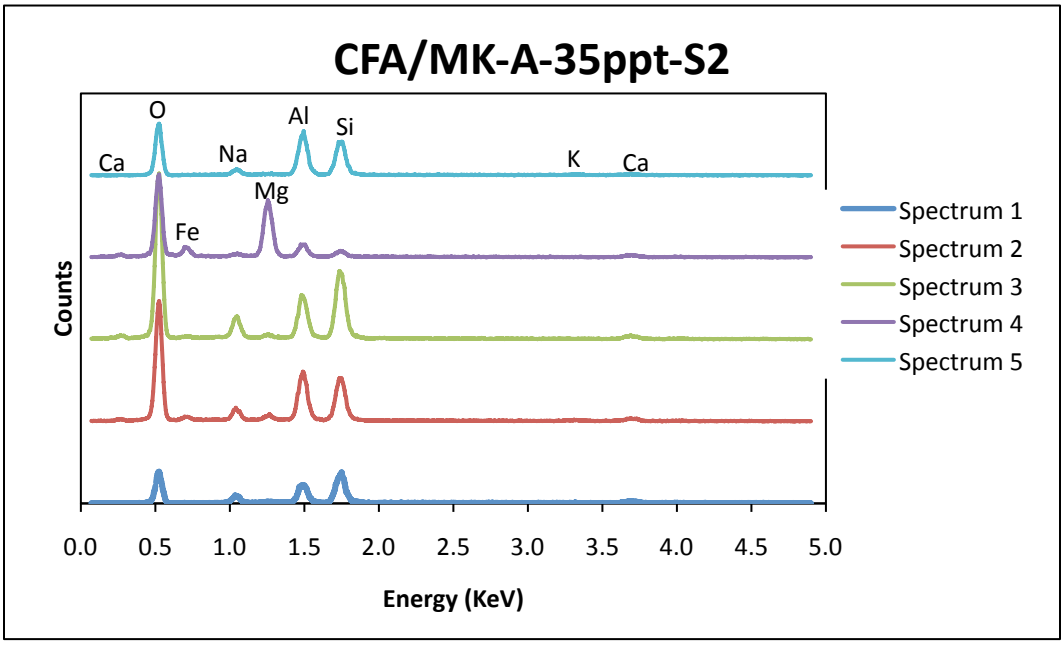

Figure 6.17 EDS spectra for sample obtained from 35 ppt geopolymer cement Specimen 2 sample.

7 SUMMARY, CONCLUSIONS, AND RECOMMENDATIONS

7.1 Summary

This thesis presents research methods and results from an investigation of the effect of immediate saline water curing on the properties of geopolymer cement. The properties investigated were unconfined compressive strength, elemental and mineral composition, and microstructure. As a source of comparison, Class G well cement was cured in the same conditions as the geopolymer cement. Preliminary laboratory work involved developing a geopolymer design mix that exhibited excellent workability and hardened strength. Various trial mixes were examined by following those previously developed in reference studies and altered accordingly depending on observed workability and cured state.

Once a final geopolymer cement design mix was selected, a curing procedure and apparatus were developed to facilitate immediate curing of the cement, cement-saline water interaction, fly ash particle retention, and specimen isolation. Once desired curing conditions were met, both the geopolymer cement and Class G cement were mixed, cast, and immediately allowed to cure for 28 days in water possessing the following salinities: 0 ppt, 15 ppt, and 35 ppt.

After the 28 days of curing the cement specimens were de-molded, allowed to dry out, and tested for unconfined compressive strength. The specimens exhibiting the highest compressive strength for each environment and cement type were further analyzed for elemental and mineral composition using XRF and XRD analytical techniques. pH of the curing water was taken prior to the start of curing and after curing

completion to further determine whether any leaching had occurred. The microstructure of the geopolymer cements that exhibited the highest strength for each environment was analyzed using SEM and EDS analytical techniques.

7.2 Conclusions

This investigation of the effect of immediate saline water curing on geopolymer cements focused on deriving geopolymer cement from an admixture of metakaolin and Class C fly ash and using Class G well cement as a reference for behavior when cured in the same conditions. The cement specimens underwent successful immediate saline water curing, within porous molds that were developed for the investigation, for 28 days.

Unconfined compression tests on the fully cured, dry, cement specimens resulted in an observed increase in strength for the geopolymer cement with increased salinity of the curing environment. The highest unconfined compressive strength was 58.5 MPa for the geopolymer cement cured in the 35 ppt condition. The Class G cement presented opposite behavior to the geopolymer cement, with an observed increase in strength with decreased salinity. The highest unconfined compressive strength was 62.9 MPa for the Class G cement cured in the 0 ppt condition.

XRF revealed the elemental compositions of the cements and their source materials. The results were used to calculate molar ratios of Si/Al and Na/Si for each specimen. For the geopolymer cement, decreased salinity of curing resulted in increased Si/Al and decreased Na/Si. While these ratios did not vary significantly for the Class G cement cured in different environments, a noteworthy difference in Si/Al between the

Class G dry mix and the cement indicated that some leaching of material occurred during water curing. Observed differences in the ratios of Si/Al and Na/Si for the geopolymer cement indicate that the rate of leaching increases when the salinity of the curing condition is decreased.

XRD revealed that the geopolymer cement was primarily composed of amorphous phases and that the geopolymer reaction had been carried out. The crystalline phases present in all three geopolymer cements were brucite, calcite, and quartz. For curing in saline conditions, intrusion of salt crystals was not prominent. More crystalline phases were observed with decreasing salinity in both the geopolymer and Class G cements. This increase in crystalline phases may be due to increase in leaching of materials with decreased salinity. This leaching may result in a reduction in reaction, resulting in an increase of crystalline phases.

pH testing of the curing waters supported the theory that the rate of leaching increases with decreasing salinity. Overall it was observed that the pH taken after the 28 days of curing increased with decreasing salinity for both cement types. When comparing the reference pH, taken prior to the start of curing, to these values it was observed that the greatest deviation from the reference pH occurred for curing waters with the 0ppt condition. This supported the theory that the rate of leaching increased with decreasing salinity.

SEM micrographs of the geopolymer cement samples indicated little difference in the microstructure of the cement cured in the different salinities. Unreacted Class C fly ash and metakaolin and partially reacted fly ash were observed in all geopolymer cements regardless of curing condition. An abnormality in the geopolymer cement matrix

indicated the presence of impurities within the metakaolin. EDS spectrums indicated that the Si/Al and Na/Si molar ratios of the geopolymer matrix followed similar trends to those observed in the XRF results.

7.3 Recommendations

One method for improving an understanding of leaching behavior is to create a cement specimen as a reference for zero leaching. This specimen would have to be cured in a sealed condition and analyzed under the same conditions as the cements from this study. By further studying the rate of leaching produced by various curing environments and its effect on the mechanical properties of the cement, additional alteration of the mix design could be performed to maximize favorable properties.

To further investigate the viability of geopolymer cement as a replacement for standard well cements, the curing condition should be additionally altered to more closely simulate the offshore conditions. Altering immediate saline water curing conditions to include higher pressure and lower temperatures would allow for a closer offshore simulation at depth. This would require further consideration into the mold materials used for immediate water curing with respect to the material properties and resilience in such environments.

Saltwater mixing of cement is a practice that is being adapted for offshore well cementing projects. An investigation into replacing RO water with saline water in the geopolymer design mix and determining the resulting effect on strength, composition,

and pore size would be advantageous in determining further applicability of geopolymer cement as well cement.

REFERENCES

Ahmaruzzaman M.(2010). "A review on the utilization of fly ash." Prog. Energ. Combust., 36(3), 327-363.

Allahverdi A., Mehrpour K.,Najafikani E. (2008). "Investigating the possibility of utilizing pumice-type natural pozzonal in production of geopolymer cement." Ceram-Silikaty, 52(1), 16-23.

American Petroleum Institute, (2010). *"Specification for cements and materials for well cementing." 10A/ISO 10426*, Washington, D.C.

ASTM Subcommittee C01.10 on Hydraulic Cements for General Concrete Construction. (2014). "*Standard specification for blended cements*." C 595/595M-14, ASTM International, Philadelphia, PA, www.astm.org

ASTM subcommittee C09.61 on Testing and strength. (2014). "*Standard test method for compressive strength of cylindrical concrete specimens." C39/39M-14, ASTM International, Section 4 Construction, Vol. 04.02 Concrete and Aggregates*, West Conshohocken, PA, www.astm.org

ASTM subcommittee C09.61 on Testing and Strength. (2012). *"Standard practice for capping cylindrical concrete specimens." C617/617M-12*, *ASTM International, Section 4 Construction, Vol. 04.02 Concrete and Aggregates*, West Conshohocken, PA, www.astm.org

ASTM. (2002). *"Standard Specification for Portland Cement." C150/C150M-12, Annual Book of Standards, 2002. Section 4 Construction, Vol. 04.01 Cement; Lime; Gypsum,* West Conshohocken, PA.

ASTM. (2011). "Standard test method for particle-size analysis of soils." D442-90, *Annual book of ASTM standards, 2011. Section 4 Construction, Vol. 04.08, Soils and Rocks (I): D420-D5876,* West Conshohocken, PA.

ASTM. (2011). *"Standard test methods for laboratory determination of water (Moisture) content of soil and rock by mass." D2216-90, Annual book of ASTM standards, 2011. Section 4 Construction, Vol. 04.08 Soil and Rock (I): D420 D5876,* West Conshohocken, PA, www.astm.org.

Atis, C. D. (2002). "High Volume Fly Ash Abrasion Resistant Concrete." J. Mater. Civ. Eng., 14(3), 274-277.

Atis, C. D., Karahan, O. (2009). "Properties of steel fiber reinforced fly ash concrete." Constr. Build. Mater., 23(1), 392-399.

Atkinson, M., and Bingman, C. (1997). "Elemental composition of commercial seasalts." J. Aquaricult. Aquat. Sci., 8(2), 39-43.

Bruant, R.G. Jr., Guswa, A.J., Celia, M.A, Peters, C.S. (2002). “Safe storage of CO_2 in deep saline aquifers” J. Environ. Sci. Technol., 36 (11), 240-245.

Cao, C., Wei, S., Qin, H. (2000). "The analysis on strength and fly ash effect of roller-compacted concrete with high volume fly ash." Cem. Concr. Res., 30(1), 71-75.

Cheng, T.W.,Chiu, J.P. (2003). "Fire-resistant geopolymer produced by granulated blast furnace slag." Miner. Eng., 16(3), 205-210.

Chesner, W., Collins, R., and MacKay, M. (1998). User Guidelines for Waste and by-Product Materials in Pavement Construction, US Department of Transportation, Federal Highway Administration, Publication No. FHWA-RD-97-1448.

Chindaprasirt, Prinya, Silva, Pre, Sagoe-Crentsil, Kwesi,Hanjitsuwan, Sakonwan. (2012). "Effect of SiO2 and Al2O3 on the setting and hardening of high calcium fly ash-based geopolymer systems." J. Mater. Sci., 47(12), 4876-4883.

Chung, C.W., Shon, C.S.,Kim, Y.S. (2010). "Chloride ion diffusivity of fly ash and silica fume concretes exposed to freeze-thaw cycles." Constr. Build. Mater., 24(9), 1739-1745.

Davidovits, J. (1976). "Solid phase synthesis of a mineral blockpolymer by low temperature polycondensation of aluminosilicate polymers." IUPAC International Symposium on Macromolecules Stockholm, Topic III, New Polymers of High Stability.

Davidovits, J. (1979). SPE PATEC '79. Society of Plastic Engineering, Brookfield Center, USA.

Davidovits, J. (1991). "Geopolymers: inorganic polymeric new materials." J. Therm. Anal., 37 1633-1656.

Davidovits, J. (1999). “Chemistry of geopolymeric systems, terminology.” In: Proc. 2nd Internat. Conf. Geopolymere ’99, 9-39.

Davidovits, J. (2008). Geopolymer chemistry and applications, 3rd Edition, Saint-Quentin, France, Ch. 1, 4-5.

Duxson, P., Fernâandez-Jimâenez, A., Provis, J., Lukey, G., Palomo, A., Deventer, J. (2007). "Geopolymer technology: the current state of the art." J. Mater. Sci., 42(9), 2917-2933.

Duxson, P., Mallicoat, S.W., Lukey, G.C., Kriven, W.M.,van Deventer, J.S.J. (2007b). "The effect of alkali and Si/Al ratio on the development of mechanical properties of metakaolin-based geopolymers." Colloids Surf. A., 292(1), 8-20.

Duxson, Peter, Provis,John L. (2008). "Designing Precursors for Geopolymer Cements." J. Am. Ceram. Soc., 91(12), 3864-3869.

Fernández-Jiménez, A,Palomo, A. (2003). "Characterisation of fly ashes. Potential reactivity as alkaline cements." Fuel, 82(18), 2259-2265.

Gao K., Wang D., Lin K.L., Shiu H.S., Hwang C.L., Chang Y.M., Cheng T.W. (2014). "Effects SiO2/Na2O molar ratio on mechanical properties and the microstructure of nano-SiO2 metakaolin-based geopolymers." Constr. Build. Mater., 53 503-510.

Giasuddin, H.M., Sanjayan, J.G.,Ranjith, P.G. (2013). "Strength of geopolymer cured in saline water in ambient conditions." Fuel, 107 34-39.

Guo X., Shi H.,Dick W.A. (2010). "Compressive strength and microstructural characteristics of class C fly ash geopolymer." Cem. Concr. Compos., 32(2), 142-147.

He, J., Zhang, J., Yu, Y., Zhang, G. (2012). "The strength and microstructure of two geopolymers derived from metakaolin and red mud-fly ash admixture: a comparative study.(Report)." Constr. Build. Mater., 30(1), 80-91.

Huntzinger, D.N., Eatmon, T.D., Present and Anticipated Demands for Natural Resources: Scientific, Technological, Political,Economic and Ethical Approaches for Sustainable Management. (2009). "A life-cycle assessment of Portland cement manufacturing: comparing the traditional process with alternative technologies." J.Clean.Prod., 17(7), 668-675.

Jarrige, A. (1971). Les cendres volantes : propriétés, applications industrielles. Eyrolles, Paris.

Li, G., Zhao, X. (2003). "Properties of concrete incorporating fly ash and ground granulated blast-furnace slag." Cem. Concr. Compos., 25(3), 293-299.

Li, Z. (2007). "Influence of Slag as Additive on Compressive Strength of Fly Ash-Based Geopolymer." J. Mater. Civil Eng., 19(6), 470-474.

Lukey, G.C., Mendis, P.A., van Deventer, J.S.J., Sofi, M. (2006). "Advances in Inorganic Polymer Concrete Technology." In Day. K. W. (Ed.) *Concrete Mix Design, Quality Control and Specification*, 3rd Edition. London, Routledge.

Malhotra, V. M., Ramezanianpour, A. A.,Mineral Sciences Laboratories (Canada). (1994). Fly ash in concrete. Natural Resources Canada, CANMET, Ottawa, Ont., Canada.

Melo, K.A.,Carneiro, A.M.P. (2010). "Effect of Metakaolins finesses and content in self-consolidating concrete." Constr. Build. Mater., 24(8), 1529-1535.

Meyer, C. (2009). "The greening of the concrete industry." Cem. Concr. Compos., 31(8), 601-605.

Mohammed, B. S., Fang, O.C. (2011). "Mechanical and durability properties of concretes containing paper-mill residuals and fly ash." Constr. Build. Mater., 25(2), 717-725.

Nasvi, M. C. M., Ranjith, P. G.,Sanjayan, J. (2013). "Effect of different mix compositions on apparent carbon dioxide (CO2) permeability of geopolymer: Suitability as well cement for CO2 sequestration wells." Appl. Energy, 114 939-948.

Nasvi, M.C.M., Ranjith, P.G., Sanjayan, J., (2012). "The permeability of geopolymer at down-hole stress conditions: Application for carbon dioxide sequestration wells." Appl. Energy, 102 1391-1398.

Palomo, A., Grutzeck, M.W., Blanco, M.T. (1999). "Alkali-activated fly ashes: A cement for the future." Cem. Concr. Res., 29(8), 1323-1329.

Rashad, A. M. (2014). "A comprehensive overview about the influence of different admixtures and additives on the properties of alkali-activated fly ash." Materials and Design., 53 1005-1025.

Roy, A., Schilling, P.J., Eaton, H.C. (1996). Alkali activated class C fly ash cement, U.S. Patent 5, 565028.

Sanna, A., Dri, M., Hall, M.R.,Maroto-Valer, M. (2012). "Waste materials for carbon capture and storage by mineralisation (CCSM) - A UK perspective." Appl.Energy, 99 545-554.

Saraswathy, V, Muralidharan, S, Thangavel, K,Srinivasan, S. (2003). "Influence of activated fly ash on corrosion-resistance and strength of concrete." Cem. Concr. Compos., 25(7), 673-680.

Somna, K., Jaturapitakkul, C., Kajitvichyanukul, P.,Chindaprasirt, P. (2011). "NaOH-activated ground fly ash geopolymer cured at ambient temperature." Fuel, 90(6), 2118-2124.

Sumer, M. (2012). "Compressive strength and sulfate resistance properties of concretes containing Class F and Class C fly ashes." Constr. Build. Mater., 34(1), 531-536.

Swanepoel, J.C., Strydom, C.A. (2002). "Utilisation of fly ash in a geopolymeric material." Appl. Geochem., 17(8), 1143-1148.

Temuujin J, van Riessen A,Williams R. (2009). "Influence of calcium compounds on the mechanical properties of fly ash geopolymer pastes." J. Hazard. Mater., 167(1-3), 1-3.

Turner, L. K. (2013). "Carbon Dioxide equivalent (CO2-e) emissions: A comparison between geopolymer and OPC cement concrete." Constr. Build. Mater., 43 125-130.

van Jaarsveld, J. G., van Deventer, J. S., Lukey,G.C. (2002). "The effect of composition and temperature on the properties of fly ash- and kaolinite-based geopolymers." Chem. Eng. J., 89(1-3), 63-73.

van Jaarsveld, J.G.S., van Deventer, J.S.J., Lorenzen, L. (1997). "The potential use of geopolymeric materials to immobilise toxic metals: Part I. Theory and applications." Miner. Eng., 10(7), 659-669.

Van Jaarsveld, J.G.S., van Deventer, J.S.J.,Lukey, G.C. (2003). "The characterization of source materials in fly ash-based geopolymers." Mater. Lett., 57(7), 1272-1280.

Verdolotti, L., Iannace, S., Lavorgna, M. ,Lamanna, R. (2008). "Geopolymerization reaction to consolidate incoherent pozzolanic soil." J. Mater. Sci., 43(3), 865-873.

Xu, H., van Deventer, J.S.J. (1999). "The geopolymerisation of alumino-silicate minerals." Int. J. Miner. Process., 59(3), 247-266.

Yeh, A.C., Bai, H. (1999). "Comparison of ammonia and monoethanolamine solvents to reduce CO2 greenhouse gas emissions." Sci. Total Environ., 228(2-3), 121-133.
Yu, Z., Ye, G. (2013). "The pore structure of cement paste blended with fly ash." Constr. Build. Mater., 45 30-35.

Zhang T.S., Yu Q.J., Wei J.X., Zhang P.P. (2011). "Effect of size fraction on composition and pozzolanic activity of high calcium fly ash." Adv. Cem. Res., 23(6), 299-307.

Zhang, G., He, J., Gambrell R.P. (2010). "Synthesis. characterization, and mechanical properties of red mud-based geopolymers." Transp. Res. Record, 2167, 1-9.